frontiers in Earth Science

ORIGINAL RESEARCH
published: 24 December 2021
doi: 10.3389/feart.2021.773819

Intermittent Growth of a Newly-Born Volcanic Island and Its Feeding System Revealed by Geological and Geochemical Monitoring 2013–2020, Nishinoshima, Ogasawara, Japan

Fukashi Maeno[1]*, *Atsushi Yasuda*[1], *Natsumi Hokanishi*[1], *Takayuki Kaneko*[1], *Yoshihiko Tamura*[2], *Mitsuhiro Yoshimoto*[3], *Shun Nakano*[4], *Akimichi Takagi*[5], *Minoru Takeo*[1,5] and *Setsuya Nakada*[1,6]

[1]Earthquake Research Institute, The University of Tokyo, Tokyo, Japan, [2]Japan Agency for Marine-Earth Science and Technology, Yokosuka, Japan, [3]Mount Fuji Research Institute, Yamanashi Prefectural Government, Fujiyoshida, Japan, [4]Geological Survey of Japan, National Institute of Advanced Industrial Science and Technology, Tsukuba, Japan, [5]Japan Meteorological Agency, Tokyo, Japan, [6]National Research Institute for Earth Science and Disaster Resilience, Tsukuba, Japan

OPEN ACCESS

Edited by:
Joan Marti,
Spanish National Research Council (CSIC), Spain

Reviewed by:
Corrado Cimarelli,
Ludwig Maximilian University of Munich, Germany
Heather Michelle Wright,
United States Geological Survey (USGS), United States

***Correspondence:**
Fukashi Maeno
fmaeno@eri.u-tokyo.ac.jp

Specialty section:
This article was submitted to Volcanology, a section of the journal Frontiers in Earth Science

Received: 10 September 2021
Accepted: 06 December 2021
Published: 24 December 2021

Citation:
Maeno F, Yasuda A, Hokanishi N, Kaneko T, Tamura Y, Yoshimoto M, Nakano S, Takagi A, Takeo M and Nakada S (2021) Intermittent Growth of a Newly-Born Volcanic Island and Its Feeding System Revealed by Geological and Geochemical Monitoring 2013–2020, Nishinoshima, Ogasawara, Japan. Front. Earth Sci. 9:773819. doi: 10.3389/feart.2021.773819

The island-forming Nishinoshima eruptions in the Ogasawara Islands, Japan, provide a rare opportunity to examine how the terrestrial part of Earth's surface increases *via* volcanism. Here, the sequence of recent eruptive activity of Nishinoshima is described based on long-term geological and geochemical monitoring of eruptive products. Processes of island growth and temporal changes in the magma chemistry are discussed. The growth of Nishinoshima was sustained by the effusion of low-viscosity andesite lava flows since 2013. The lava flows spread radially with numerous branches, resulting in compound lava flows. Lava flows form the coherent base of the new volcanic edifice; however, pyroclastic eruptions further developed the subaerial volcanic edifice. The duration of three consecutive eruptive episodes decreased from 2 years to a week through the entire eruptive sequence, with a decreasing eruptive volume and discharge rate through time. However, the latest, fourth episode was the most intense and largest, with a magma discharge rate on the order of 10^6 m^3/day. The temporal change in the chemical composition of the magma indicates that more mafic magma was involved in the later episodes. The initial andesite magma with ~60 wt% SiO_2 changed to basaltic andesite magma with ~55 wt% SiO_2, including olivine phenocryst, during the last episode. The eruptive behavior and geochemical characteristics suggest that the 2013–2020 Nishinoshima eruption was fueled by magma resulting from the mixing of silicic and mafic components in a shallow reservoir and by magma episodically supplied from deeper reservoirs. The lava effusion and the occasional explosive eruptions, sustained by the discharge of magma caused by the interactions of these multiple magma reservoirs at different depths, contributed to the formation and growth of the new Nishinoshima volcanic island since 2013. Comparisons with several examples of island-forming eruptions in shallow seas indicate that a long-lasting voluminous lava effusion with a discharge rate on the order of at least 10^4 m^3/day (annual average) to 10^5 m^3/day (monthly average) is

required for the formation and growth of a new volcanic island with a diameter on km-scale that can survive sea-wave erosion over the years.

Keywords: volcanic island, Nishinoshima, lava flow, pyroclast, monitoring, andesite

1 INTRODUCTION

Volcanic eruptions occur in shallow-water environments in active volcanic regions, such as at convergent plate boundaries, and in hot spots and rift zones in and along oceanic plates. These submarine eruptions often result in a change in the eruptive environment from submarine to subaerial and the production of a new island. The emergence and growth of a new volcanic island provide a rare opportunity to examine how the terrestrial part of the Earth surface increases *via* volcanism. Such events also provide fundamental knowledge concerning the very early stages of growth of a large volcanic island edifice. Our current understanding is limited because only a few examples of volcanic island formation have been documented in historical times. One famous example is Surtsey in Iceland in the 1960s, where the creation and growth of a new volcanic island were observed and summarized in detail (e.g., Thorarinsson et al., 1964; Thordarson and Sigmarsson, 2009). Although submarine eruptions in shallow seas have been recently observed in volcanically active regions, e.g., the Zubair archipelago in the southern Red Sea (Xu et al., 2015) and the Tonga archipelago (Cronin et al., 2017), detailed observations are rarely achieved because tiny new islets can easily be eroded by waves and disappear in a short period without the supply of a large volume of magma to the surface. Even in the Japanese archipelago, only two cases have created new long-lasting (decadal-year-old) islands in historical times before the 2013–2020 Nishinoshima eruption: the eruptions in Nishinoshima, Ogasawara, from 1973 to 1974

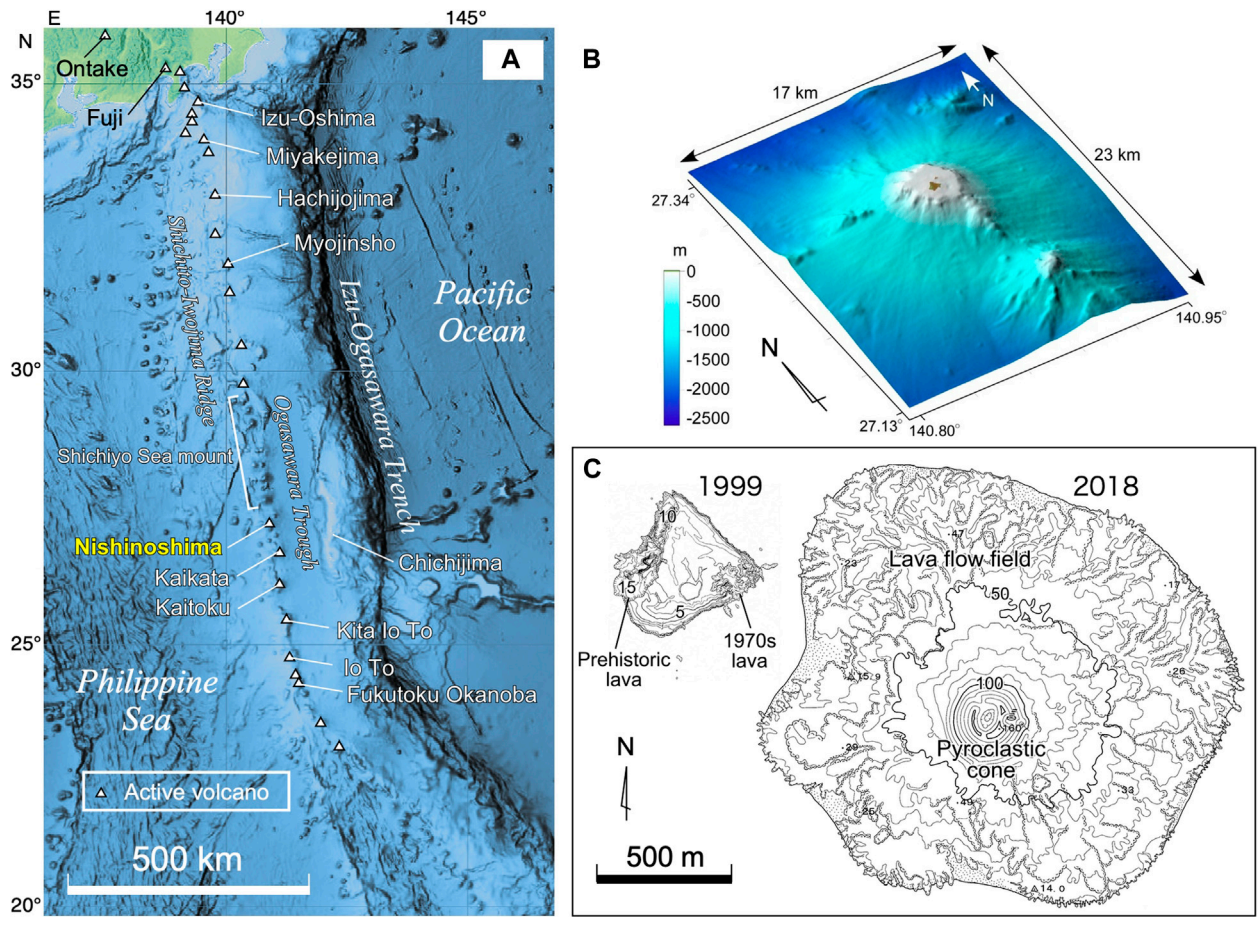

FIGURE 1 | (A) Location map of Nishinoshima. Bathymetry data from NOAA's National Centers for Environmental Information. **(B)** Bathymetry around Nishinoshima before the recent eruptions. Bathymetry data (M7023 ver 2.0) from the Marine Information Research Center, Japan Hydrograph Association. **(C)** Topographical maps drawn before and during the recent eruptions obtained by the Japan Coast Guard in 1999 (Umino and Nakano, 2007) and by the Geospatial Information Authority of Japan in 2018, respectively. The unit of height is meters for topographic contours, and the zero contour represents sea level.

FIGURE 2 | Photos of the recent Nishinoshima eruptive sequence. **(A)** Very initial phase of the volcanic-island formation with phreatomagmatic explosions, taken on November 21, 2013. The old Nishinoshima island is on the left. **(B)** Surtseyan eruption with "cocks' tail" jets, taken on November 21, 2013. **(C)** A small cone ejecting ballistics, which made splashing of water, taken on November 23, 2013. **(D)** The new growing island (below), approaching the old island (above), taken on December 20, 2013. **(E)** The new island with a Strombolian eruption almost contacting the old island, taken on December 25, 2013. **(F)** Lava flows in the northeast, contacting seawater, generating smoke, and reclaiming land, taken on March 4, 2014. **(G)** The pyroclastic cone and part of the old island, late Episode 1, taken on November 17, 2015. **(H)** Lava flows in the southwest spreading into the sea during Episode 2, taken on April 21, 2017. **(I)** Strombolian eruption and lava flows at night during Episode 2, taken on May 25, 2017, by H. Abe. **(J)** Lava flow effusing from the central vent to the south during Episode 3, taken on September 8, 2018. **(K)** Ash plume observed during late Episode 4, taken on July 30, 2020. **(L)** Tephra blanket (pyroclastic fallout deposits) from Episode 4, covering lava flows and smoothing the surface, taken on July 30, 2020. **(M)** The ~250-m-high pyroclastic cone that grew during Episode 4, taken on December 23, 2020, from the west.

(previous activity) (Ossaka et al., 1974; Ossaka, 1991) and in Showa Iwo-jima, southern Kyushu, from 1934 to 1935 (Tanakadate, 1934; Maeno and Taniguchi, 2006). Furthermore, many active island or submarine volcanoes exist in remote areas, making it difficult to comprehensively observe detailed processes.

Nishinoshima in Ogasawara, Japan, has continued its eruptive activity through four eruptive episodes since 2013 and this latest

activity created a new volcanic island (**Figures 1**, **2**). Episode 1 occurred from November 2013 to December 2015, as summarized by Maeno et al. (2016); then, the eruptive activity continued intermittently. Episodes 2 and 3 occurred in April–August 2017 and July 2018, respectively, (Kaneko et al., 2019). Then, Episode 4 occurred from December 2019 to August 2020. The size of the new island increased incrementally to 2.5 km × 2.5 km at the end of the most recent Episode 4 in 2020. This series of volcanic activity at Nishinoshima provides an important opportunity to study the birth, growth, and development of a new volcanic island. Several previous studies deal with specific topics concerning these recent Nishinoshima eruptions (Maeno et al., 2016; Sano et al., 2016; Shinohara et al., 2017; Maeno et al., 2018; Takeo et al., 2018; Kaneko et al., 2019; Tamura et al., 2018; Baba et al., 2020; Tada et al., 2021); however, the entire sequence of these eruptions, including the variation in the eruptive style and magma chemistry, has not yet been summarized and discussed. In this paper, we study the 2013–2020 Nishinoshima eruption and discuss the formation process for the new volcanic island and the magma supply system beneath the island based on time series of geological and geochemical data obtained *via* remote observations and land surveys at the volcano.

2 NISHINOSHIMA VOLCANO

Nishinoshima is located approximately 1,000 km south of Tokyo and 130 km west of Chichijima, Ogasawara (**Figure 1**). It is an active volcano that consists of a volcanic front (Shichito-Iwojima Ridge) of the Izu-Bonin arc, trending in the north–south direction parallel to the Ogasawara Trench. Nishinoshima consists of a main peak that appears as an island and two submarine peaks that are located west and south of the island. There is a small cone on the northeast flank of the main peak, which may be a satellite cone (Yuasa et al., 1991). The volcanic activity in this region is caused by the subduction of the Pacific Plate beneath the Philippine Sea Plate. North of Nishinoshima, large submarine stratovolcanoes, with basal diameters of 20–30 km, reaching heights of 2,200–2,800 m above their base, form the chain called the Shichiyo Seamount (Yuasa et al., 1991; Ishizuka et al., 2007). South of Nishinoshima, the volcanic front includes the Kaikata and Kaitoku seamounts and the volcanic islands of Kita Io To, Io To, and Minami Io To. Although there are studies on magma genesis related to subduction in this region (Yuasa and Nohara, 1992; Ishizuka et al., 2007; Sano et al., 2016; Tamura et al., 2018), the detailed eruptive histories of these active volcanoes, including Nishinoshima, have not been established because of the submarine nature of the major volcanic products and edifices.

Prior to 1973, Nishinoshima was a tiny island consisting of andesite lava, which was the remnant of an old volcanic edifice of unknown age with a length of 200 m, width of 50 m, and height of 25 m extending in the northeast–southwest direction (**Figure 1**), being this the tip of a much larger submarine volcanic edifice. Before the recent 2013 eruptive event, the volcanic eruptions occurred from 1973 to 1974 were the only known historical eruptive activity at Nishinoshima since its discovery in 1702 (Aoki and Ossaka, 1974). During 1973–1974, a new island was formed to the southeast, offshore of the old Nishinoshima island. This was likely the latest eruptive episode experienced by the volcano. However, the small magnitude of the eruptions and the subsequent erosion and sedimentation of reworked volcanic material, did change the dimension of the island considerably (Ossaka, 1991). Although the magma erupted during the 1970s was andesitic in composition, it did slightly differ from the composition of the prehistoric lava, as shown later.

Immediately prior to 2013, the Nishinoshima island consisted of three major areas: a western hill consisting of prehistoric lavas with an unknown age, a height of 25 m, and a flat top; younger lava flows erupted from 1973 to 1974 to the east; and a middle low land consisting of reworked sand and gravel (Umino and Nakano, 2007). The island at this time had a trapezoidal shape with a maximum length of ~600 m and an extension of c.a. 0.2 km^2 (**Figure 3**). Although there are no historical records of eruptions, exception made for those in the 1970s and 2010s, the size of the entire Nishinoshima edifice, which elevates more than ~2,500 m from the sea bottom, indicates that this volcano must have experienced many repeated magmatic eruptions over a long period of time.

3 MATERIALS AND METHODS

3.1 Remote Surveys

Throughout the four episodes of the 2013–2020 Nishinoshima eruption, remote observations from satellites, airplanes, and research vessels were used to monitor the volcano. Not only optical satellite images but also synthetic aperture radar satellite data (TerraSAR-X, ALOS-2) were used to constrain the temporal changes in the eruption processes. The SAR observations are not affected by clouds or eruption plumes because they use electromagnetic waves with long wavelengths. Such observations of a fixed point in a fixed interval allow analyses of the detailed growth process *via* comparisons of time-series images (Maeno et al., 2016; Kaneko et al., 2019[1]). The airplanes (operated by Asahi Shimbun, Yomiuri Shimbun, and Mainichi Shimbun) and research vessels (*Kairei, Natsushima, Shinseimaru, Keifumaru, and Ryofumaru*) were occasionally used for visual observations of the eruptions on-site and to confirm observations from satellites. The research vessels were also used to collect ash samples during the eruption. The remotely controlled aerial vehicles, which were operated from the research vessels, were used to observe the eruptive activities and geological features in more detail, as well as to obtain ash and lapilli samples from the volcanic edifice (**Table 1**). The remote observations by the Japan Coast Guard (JCG), the Japan Meteorological Agency (JMA), and the Geospatial Information Authority of Japan (GSI) were considered in construction of the eruption process. On the basis of these surveys and data, the surface morphology, area, volume, discharge rate, and their changes were quantitatively estimated and used to explore the origins of their variations.

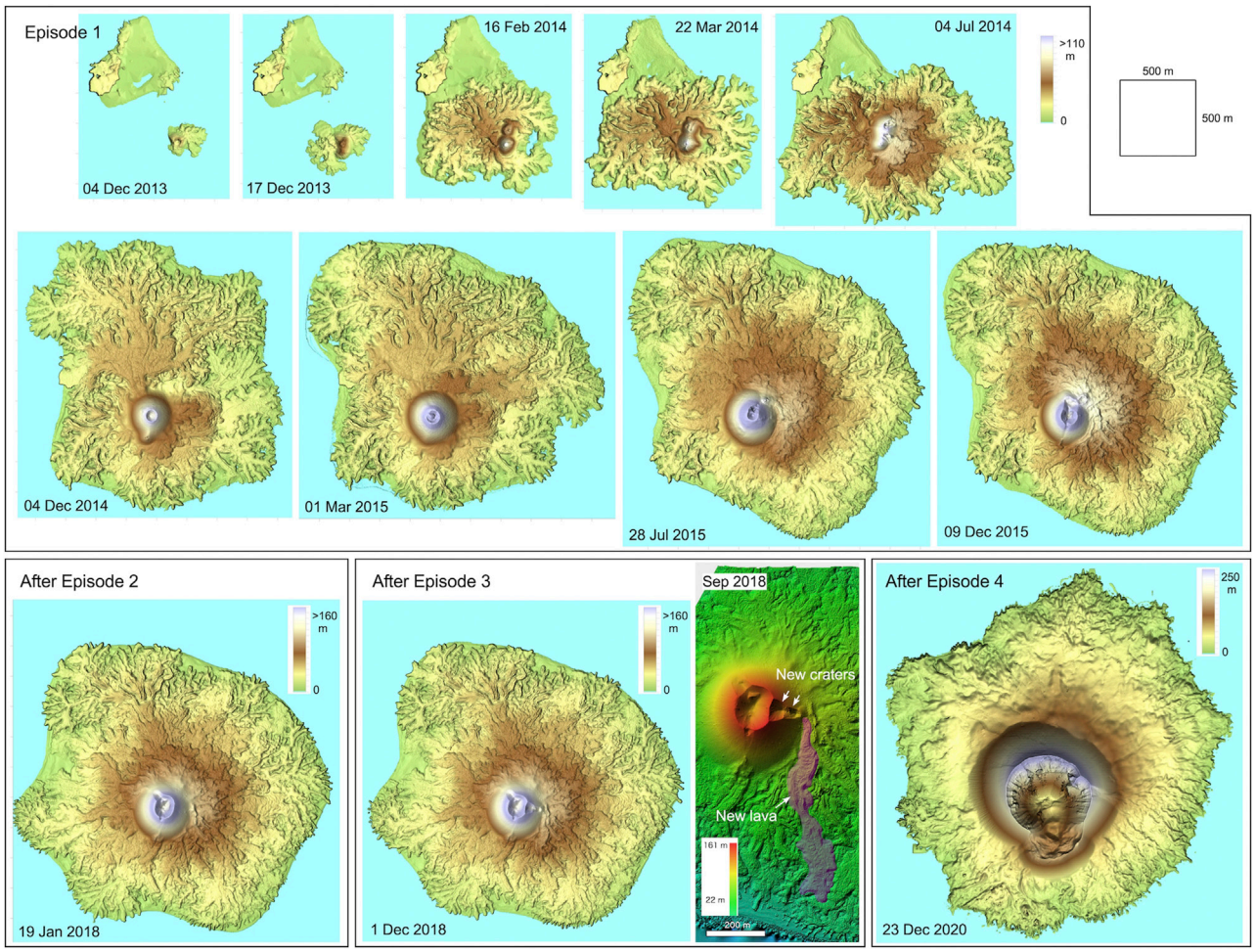

FIGURE 3 | Temporal change in the topography of Nishinoshima since the beginning of the recent eruptions in 2013. The original topographic data for 2013–2018 were provided by the Geospatial Information Authority of Japan. The detailed topography of the central cone and new lava after Episode 3 and the topography of the entire island after Episode 4 were obtained *via* aerial drone surveys.

TABLE 1 | Samples obtained from Nishinoshima and sampling methods.

Episode	Eruption date	Sampling location	Sample type	Sampling date	Sampling methods
1	2014-Jan to 2015-Nov	West coast	Lava, bomb, lapilli	2016/10/20, 21	Land survey, R/V Shinseimaru (KS16-16)
1	2014–2015	Western foot of cone	Lapilli	2016/6/7, 8	UAV from R/V Keifumaru (KS16-05)
1	2015-Feb-27	Off shore	Ash	2015/2/27	On R/V Kairei (KR15-03)
1	2015-Jun-15	Off shore	Ash	2015/6/15	On R/V Natsushima (NT15-E02)
1	2015-Jun to Jul	South coast	Lava	2016/10/28	Land survey by JCG (sampled by JCG)
2	2017-May-28	Off shore	Ash	2017/5/28	On R/V Keifumaru (KS17-04)
2	2017-Apr to Aug	Summit	Lapilli	2018/5/30	Drone from R/V Ryofumaru (KS18-04)
2	2017-Apr to Aug	West coast	Lava	2019/9/3, 4	Land survey (CSR)
2	2017-Apr to Aug	Southwest coast	Lava	2019/9/5	Land survey (CSR)
3	2018-mid Jul	Summit	Lapilli	2018/9/8	Drone from R/V Keifumaru (KS18-07)
3	2018-mid Jul	Summit	Lapilli	2019/6/8	Drone from R/V Ryofumaru (KS19-05)
4	2020-end of Jun	Southwest coast	Lapilli (scoria raft)	2020/12/23	Drone from R/V Kairei (KR20-E06)
4	2020-eartly Jul	West coast	Lapilli, ash	2020/12/21	Drone from R/V Kairei (KR20-E06)
4	2020-Jul-11	Off shore	Ash	2020/7/11	On R/V Ryofumaru (sampled by JMA)
4	2020-Jul-20	Off shore	Ash	2020/7/20	On R/V Keifumaru (sampled by JMA)

JCG, Japan Coast Guard; JMA, Japan Meteorological Agency; JAM, Japan Agency for Marine-Earth Science and Technology; CSR, comprehensive scientific research operated by the Ministry of the Environment Japan; KS (KR, NT) xx-xx: Cruise number.

3.2 Land Surveys

During the 2013–2020 eruption, for safety reasons, access to Nishinoshima was strictly prohibited, with the restricted area being larger than the island. Therefore, remotely controlled aerial vehicles were the only method available to directly approach the island for observation and sampling. However, during the quiet periods, the restricted area was reduced to 0.5 km from the center of the island, making it possible to conduct land surveys. In October 2016 and September 2019, we carried out land surveys on the western and southwestern coasts, where sandy and gravelly beaches had developed. A multidisciplinary research team including volcanologists, biologists and zoologists participated to the survey. To avoid contamination by external species and to conserve the primitive environmental conditions, all scientists carefully followed the guidelines suggested by the Ministry of the Environment, Japan. On the island, we took rock samples and surveyed the distribution and structure of the lava flows and tephra deposits to characterize the eruptive processes. We sampled rocks whose time of emplacement could be estimated using aerial and satellite images; this allowed us to construct the time-series variation of the chemical compositions of the lava flows and some ballistic ejecta.

3.3 Chemical Composition Analyses

Eruptive products from each episode during 2013–2020 were sampled on land and offshore Nishinoshima by the research vessels, remotely controlled aerial vehicles, and land surveys as mentioned above. The sampling methods and analyzed samples are summarized in **Table 1**. We performed microscope observations, whole rock major and trace element analyses using X-ray fluorescence spectrometry (ZSX Primus II, Rigaku Co., Ltd., Tokyo, Japan), and groundmass and mineralogical analyses using an electron probe micro-analyzer (JXA-8800R, JEOL Ltd., Tokyo, Japan), with an acceleration voltage of 15 kV, a beam current of 12 nA, and a beam diameter of 10 μm, at the Earthquake Research Institute, University of Tokyo.

4 RESULTS

4.1 Outline of the Nishinoshima Eruptive Episodes Since 2013

4.1.1 Episode 1: 2013–2015

The latest eruptive episode began in the shallow sea ~300 m southeast offshore the previous Nishinoshima island in November 2013. The eruption was first noticed in aerial observations by the Japan Marine Self-defense Force on November 20. The depth of the eruptive center was ~30 m below sea level, and its location corresponded to one of the vents formed during the activity in the 1970s. When the eruption was reported, a new islet with a small pyroclastic cone, 150 m × 80 m in size, had already formed. The date of the beginning of the eruption is unknown; however, thermal anomaly data from Moderate Resolution Imaging Spectroradiometer satellite observations suggest that the eruption began in early November 2013. At the beginning of the eruption, magma-water interactions produced characteristic "cock's tail" explosive jets and was classified as a Surtseyan-type eruption (**Figures 2A,B**). The new island with its littoral pyroclastic cone rapidly grew by the effect of continuous eruptions in the shallow marine environment.

In late November, the eruptive style changed to Strombolian with lava flows, likely as a result of the rapid growth of the new islet, which may have prevented seawater accessing to the ascending magma (**Figure 2C**). The new islet grew *via* the continuous effusion of lava, which reclaimed the shallow sea and rapidly increased the size of the pyroclastic cone (**Figures 2D**, **3**). The pyroclastic cone was formed by ballistically ejected coarse clasts, including fluidal meter-sized bombs, from Strombolian explosions and by their rolling, which resulted in symmetrical shape with the angle of repose. In late December, the islet connected to the previous Nishinoshima island (**Figure 2E**) and grew further by emplacement of new lava flows and further growth of its pyroclastic cone (**Figure 2F**). By October 2014, most of the old island was covered by new products, except a very small plateau of the prehistoric lava to the west. Also most of the small reefs to the northeast and south were covered by new lava flows by 2015.

New lava flows then further extended the area of the new island, changed their flow direction, and formed the new Nishinoshima island, with a diameter of approximately 2 km (2.7 km^2 in area) and a height of ~150 m (**Figures 2G**, **3**, **4**). Just before this eruptive episode ended, the style of the explosions changed from prevalently Strombolian to Vulcanian. Discrete explosions produced large ballistic blocks and slightly reduced the height of the cone (**Figure 4**). The frequency of the Vulcanian explosions decreased, and the activity finally ceased at the end of 2015. After this first episode, Nishinoshima was quiet for approximately 16 months, during which the first land survey was made in October 2016.

4.1.2 Episode 2: 2017

On April 20, 2017, an eruption was confirmed through aerial observations by JCG. As in Episode 1, the activity was characterized by Strombolian activity with lava flow effusions (**Figures 2H,I**). The lava flows headed west, preferentially along topographic lows. Thermal anomalies were detected by the Himawari-8 satellite at 11:50 Japan Standard Time (JST) on April 17, and acoustic signals and intermittent tremors were detected by a seismo-acoustic station starting at 7:37 JST on April 18. Therefore, this episode is thought to have started on April 17, 2017 (Takeo et al., 2018; Kaneko et al., 2019).

In 1 week, the area covered by new lava and the additional erupted volume had reached 2.4×10^4 m^2 and 1.0×10^6 m^3, respectively. The magma discharge rate during this period was estimated to be 1.9×10^5 m^3/day on average, smaller than the values recorded during Episode 1 (**Figure 4**). This eruption continued until August 2017 and increased the land area to the west and the southwest (**Figure 3**). Although the erupted volume of this episode was smaller than that of Episode 1, due to its shorter duration, the eruptive style was nearly the same, producing Strombolian explosions and lava effusions. The Vulcanian-type explosions were also observed in the late of this episode. The area of the island reached a total of ~2.9 km^2, and

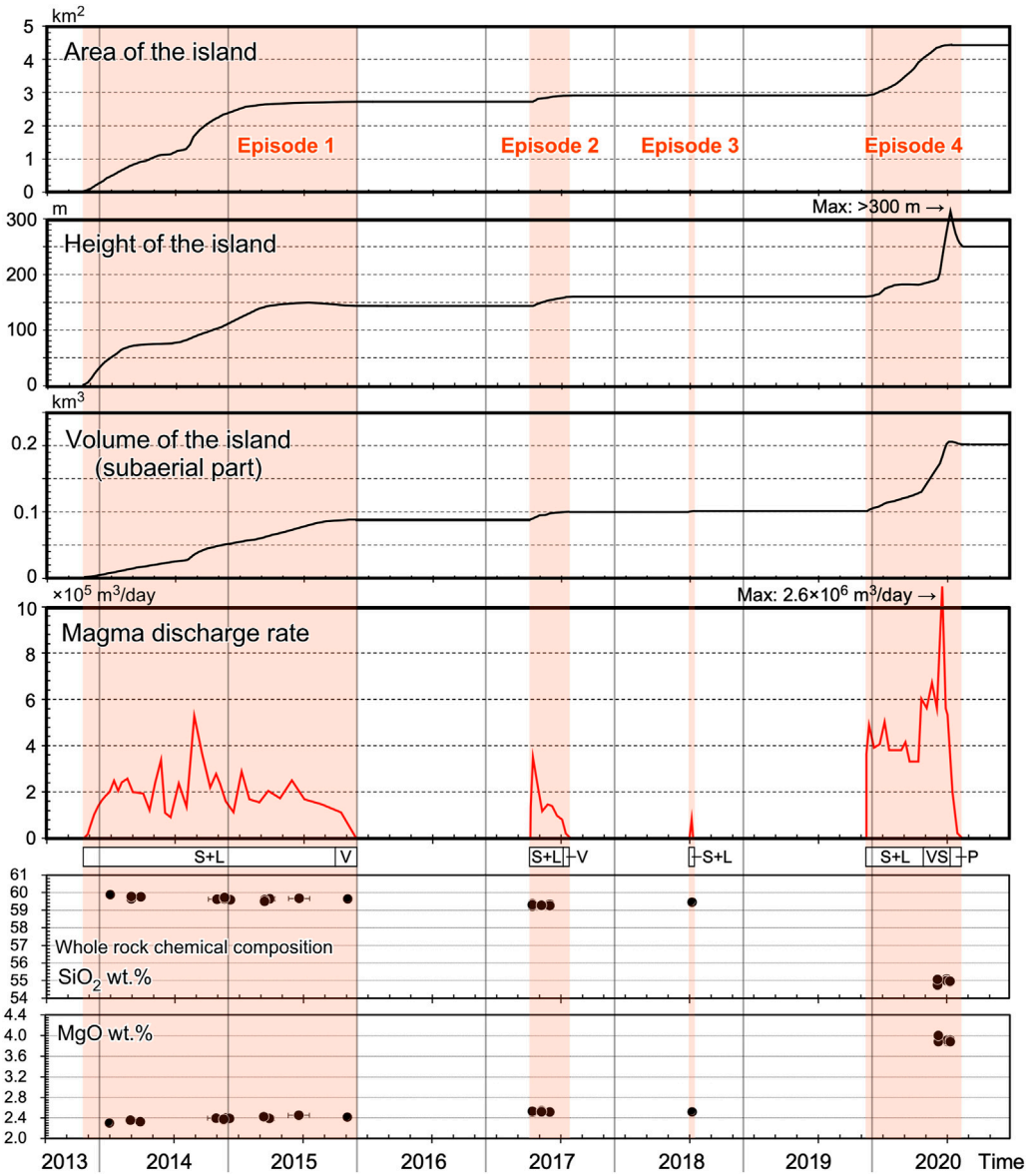

FIGURE 4 | Changes in the area, height, and volume (subaerial part) of the new island, magma discharge rate, and representative whole rock major element chemical compositions (SiO_2 and MgO) of the erupted magma during the four recent Nishinoshima eruptive episodes. Major eruption styles are also indicated below magma discharge rate: S, Strombolian; V, Vulcanian; L, Lava flow; VS, Violent Strombolian; P, Phreatomagmatic.

the height of the cone reached ~160 m (**Figure 4**). During this 4-month period, the prehistoric lavas were partially buried by new lava flows. The 2016 land survey points and a seimo-acoustic station on the west coast were also buried.

4.1.3 Episode 3: 2018

This episode began on July 12, 2018 and ceased within a week. It was characterized by Strombolian activity and lava effusion and had a much smaller scale (shorter duration and smaller volume) than that of Episode 2. New craters were produced on the eastern side of the cone, and lava exiting the cone was directed to the south (**Figures 2J**, **3**). This small-scale single-lobe lava flow did not reach the southern coast only affecting a small part of the eastern and the southern sides of the island, thus leaving the total area of the island unchanged (**Figure 4**). The additional erupted volume of the new lava was estimated to be ~2.5×10^5 m^3. If we assume that the effusive activity lasted less than a week, the magma discharge rate for the lava was $3–4 \times 10^4$ m^3/day (**Figure 4**), which is smaller than those of Episodes 1 and 2. After Episode 3, the volcano became quiet. During this period, we carried out a second land survey in September 2019.

4.1.4 Episode 4: 2019–2020

Episode 4 began in early December 2019, just 3 months after the second land survey. The eruption followed a similar pattern to the

previous episodes in its early months, being characterized by Strombolian eruptions and lava effusion with a discharge rate on the order of 10^5 m^3/day. However, the eruptive style changed dramatically from late June to early July 2020. The recent eruptive activity at Nishinoshima had mainly produced lava flows and intermittent Strombolian eruptions; however, during this period, explosive activity characterized by lava fountains and dark-colored ash plumes, similar to those often observed at basaltic volcanoes such as Etna and Hawaii, were reported by a JCG airplane and a JMA vessel. Satellites also detected an extended ash plume larger than those previously observed. From early June 2020, the height of the eruption column reached 2–6 km (~8 km in maximum on July 4, 2020), based on satellite data (Yanagisawa et al., 2020). The pyroclastic material produced by the prevalent explosive activity rapidly increased the height of the central cone to more than 300 m, as well as its diameter. Furthermore, the southern part of the cone was eventually destroyed by the issuing of new lava flows. Large blocks and fragments, that had originally made up the cone, were rafted toward the sea by the lava flows. During this period, the magma discharge rate was on the order of 10^6 m^3/day, based on thermal anomaly data captured by Himawari-8 and optical satellite images (**Figure 4**)[1]. This discharge rate was the highest recorded for Nishinoshima since 2013. After this most intense phase of Episode 4 in the middle of July 2020, the activity decreased and the eruptive style changed to continuous and vigorous ash emission. A large, light-gray colored eruptive plume was produced during this stage (**Figure 2K**), and associated fine ash entirely covered the new island (**Figure 2L**). No thermal anomalies were detected during the ash plume stage. Our later drone survey and sampling of the deposit confirmed that the topmost part of the deposits from this stage is characterized by consolidated and aggregated fine ash. These observations indicate that fragmentation mechanism that promotes finer granulation, possibly such as magma–water interactions, was involved in generating fine ash, although a thorough textural analysis of the tephra is needed to clarify its mechanism. This type of change in the eruptive style had never occurred during the past eruptive activity at Nishinoshima. However, a similar explosive activity had characterized the later explosive phase of the 2000 Miyakejima eruption, where large amounts of fine ash were generated by phreatomagmatic activity (Nakada et al., 2005). In summary, Episode 4 was first characterized as Strombolian with lava effusion, then lava-fountain eruptions, and lastly ash emission likely generated by phreatomagmatic eruptions. A more detailed sequence of this episode captured by satellites is summarized by[1]. The area of the island, at this point, had increased from 2.9 to 4.4 km^2, and its volume increased from ~0.1 to ~0.2 km^3 (**Figure 4**). The old 160-m-high pyroclastic cone was destroyed, and a new cone had grown up to a height of 250 m (**Figure 2M**). The crater diameter had been enlarged from 150 to 570 m, and the elevation of the crater floor had dropped to ~50 m above sea level. The uneven terrain of the lava flows was flattened by the tephra deposition (**Figure 3**). The change in the eruptive style in Episode 4 was due likely to the change in the magma composition from andesite to basaltic andesite, as shown later, and to the enlargement and deepening of the central crater, which resulted in magma–water interactions. The 2019 land survey points (Maeno and Yoshimoto, 2020) and the seimo-acoustic station installed during the 2019 land survey (Ohminato and Watanabe, 2020) on the west coast were buried by the new lava flows during the earlier eruptive phase.

4.2 Constraints From Remote Observations

The magma discharge rate, estimated based on the morphological changes of the island, was approximately 2.0 × 10^5 m^3/day (2.3 m^3/s) on average during Episode 1. The order of magnitude of the magma discharge rate (~10^5 m^3/day) was similar for all episodes, except Episode 3. In fact, the new island had grown stepwise with magma discharge rate fluctuations since the beginning of Episode 1. In September 2014, the magma discharge rate reached ~5.0 × 10^5 m^3/day and the northern part of the island increased very rapidly its extension (**Figure 4**). An estimation of the magma discharge rate based on the morphological change was used to correlate the magma discharge rate and the satellite-obtained thermal anomaly data (Kaneko et al., 2019). For Episode 4, the temporal variation of the magma discharge rate was estimated based on both the morphological change and the correlation between the magma discharge rate and the thermal anomaly data[1]. By the middle of June 2020, the magma discharge rate was estimated to be on the order of 10^5 m^3/day, as in earlier episodes; however, it increased to 10^6 m^3/day during the lava-fountain eruptions in June and July 2020.

Remote observations captured the dynamic behavior of the lava flows. Newly formed lava flows branched repeatedly, resulting in the formation of multiple lobe structures (**Figure 3**). This type of lava flow structure is referred to as compound lava flows (Walker, 1971; Kilburn and Lopes, 1988; Calvari et al., 2002). Analyses of satellite data confirmed that the lava flow fronts slowly advanced with a maximum speed of ~20 m/day during Episode 1. Groups of neighboring lava lobes were often inflated with time, suggesting that the lobes were interconnected and pressurized by a further supply of low-viscosity magma beneath the solidified crust (Maeno et al., 2016).

According to the aerial observations, large amounts of steam rose from the lava flow front that entered the sea. The flow front rapidly cooled as it came into contact with the seawater, and was brecciated, or auto-brecciated by the motion of the lava flow. On the surface of the lava lobes, which had already ceased to move, clefts developed, parallel to the flow direction and gradually opened and enlarged with time. These clefts were visually detected by airplanes and research vessels, as well as by land surveys, and are interpreted as being lava inflation clefts (Walker, 1991; Hon et al., 1994), which are thought to form *via* the inflation and breakage of the solid lava

[1]Kaneko, T., Maeno, F., Ichihara, M., Yasuda, A., Ohminato, T., Nogami, K., et al. (in review). Episode 4 (2019-2020) Nishinoshima Activity: Abrupt Transitions in the Eruption Style Observed by Image Datasets from Multiple Satellites. Earth Planet. Space.

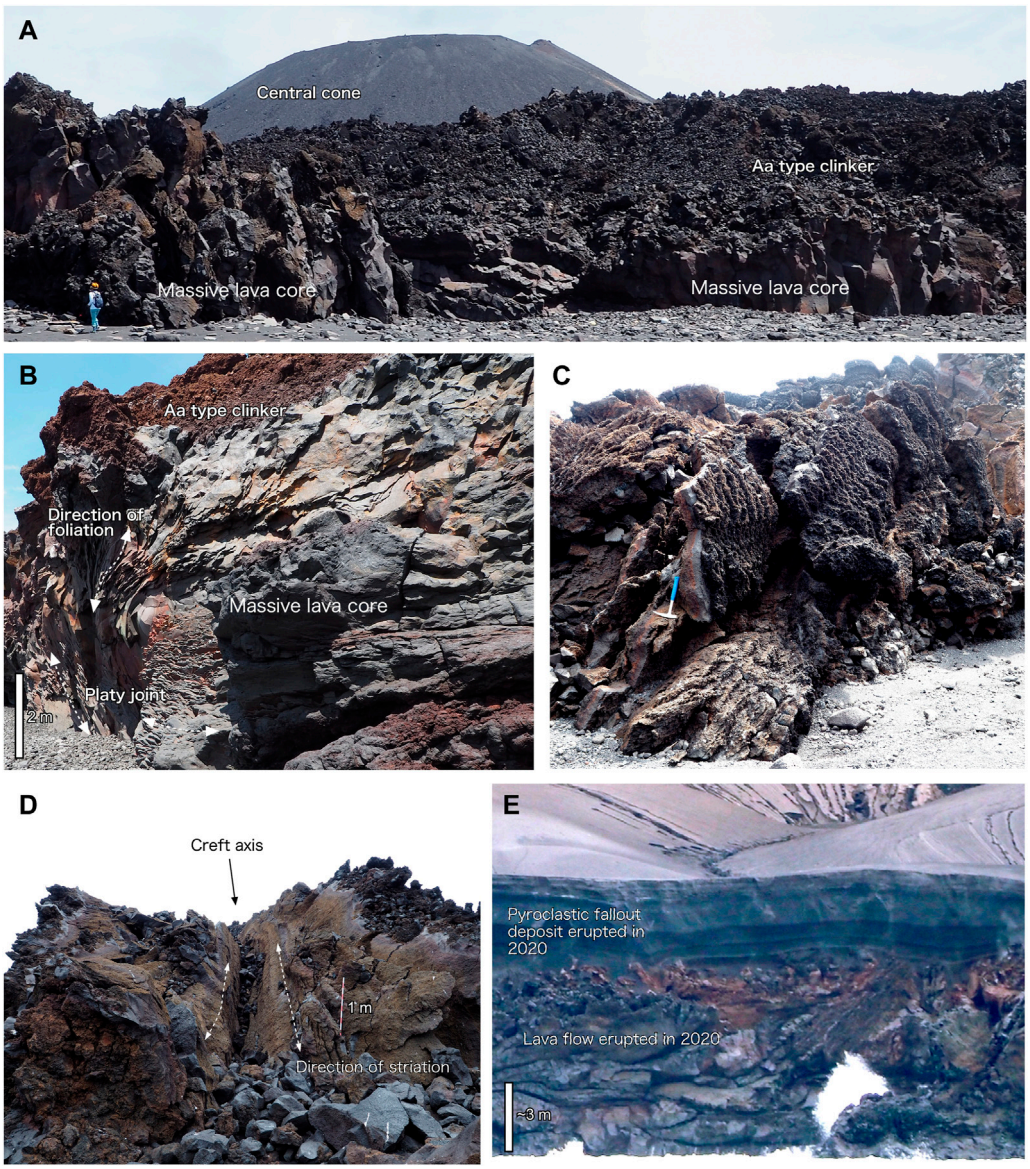

FIGURE 5 | Geological features formed by the recent Nishinoshima eruptions. **(A)** Lava flow field in the southwest of the island. The massive part of the lava (a few meters thick) is covered by aa-type clinker. **(B)** Typical massive andesite lava exposing an onion-like internal structure at a sea cliff. The platy joint developed and surrounds the core of the massive lava lobe. **(C)** Vesiculated lava clinker consisting of an andesite lava flow surface with fine protrusions. **(D)** Inflation cleft developed on the lava lobe. The black arrow shows the axial trough of the cleft, from which massive lava is thought to have fractured and opened to the left and right, as the result of inflation due to increased internal pressure during lava flowage. **(E)** Cross section of stratified pyroclastic fallout tephra deposits from late Episode 4, covering lava flows effused in early Episode 4, observed on the northwestern side of the island. The thickness of the deposit is > 3 m. Photos **(A–D)** were taken during the September 2019 land survey, and photo **(E)** was taken from research vessel *Kairei* in December 2020.

surface because of increases in the internal pressure caused by the continuous supply of still-molten lava.

The coasts of the new Nishinoshima island just after the lava emplacement in each eruptive episode were steep and rocky and consisted of irregular-shaped and complicated patterns reflecting the emplacement of multiple lava lobes. However, the shape of the island has been smoothed by erosion and the sedimentation of reworked materials and has changed with time to form a gravelly and sandy beach. On the western and northern sides of the island, a wide beach developed as the result of the competition between erosion and sedimentation.

4.3 The 2016 and 2019 Land Surveys

4.3.1 Lava Flows

The morphology, internal structure, and distribution of the lava flows were investigated along the western and southwestern coasts. There, the massive dense interiors of the lava effused during

Episodes 1 and 2 have been exposed by wave erosion. Some of them show platy, circularly developed cooling joints surrounding the massive core of the lava lobe (**Figures 5A,B**). North of the western coast, the lava shows cooling joints with a glassy surface, indicating rapid quenching of the lava flows operated by the seawater (Maeno et al., 2017). The lava surface is composed of several types of blocky or aa-type clinker (**Figures 5A,B**): a glassy type with black to dark gray colors, partially reddish due to oxidation; a massive pumiceous and dense type; and a flat-shaped type with a rough surface and fine protrusions (**Figure 5C**). Lava inflation clefts, inferred from satellite images, were also observed at several locations on the Episode 1 and 2 lava lobes (**Figure 5D**). These clefts are more prominent in the western and southwestern base of the cone and expose the massive dense interiors of the lava. We confirmed that the geological features, such as the lava-inflation clefts, internal structure of the lava lobes, and surface morphology, observed in the products of the Episode 1 were very similar to those produced during Episode 2.

4.3.2 Tephra

Before Episode 4, the flat top surface of the prehistoric lava, ~600 m from the vent, was the only place where tephra deposits could be preserved. The 2016 land survey confirmed the presence of ~10-cm-thick pyroclastic fallout deposits on the soil on the old flat lava surface. The lowermost part of the tephra layer is coarse ash mixed with fresh scoria lapilli (less than 1-cm diameter), the middle part of the deposit is composed of gray ash, and the uppermost part of fine laminated ash. This fallout deposit is thought to be derived primarily from the Episode 1 Strombolian activity. Ballistic bombs with >10-cm in diameter are also present on top of the prehistoric lava and surrounding coastal area. These bombs resulted from the Vulcanian activity in the later stage of Episode 1; during this period, JCG observed large bombs ejected toward the west, some of which crossed over the coastline and hit the sea surface causing splashing of water. The 2019 land survey confirmed that the pyroclastic fallout deposits on the old flat lava surveyed in 2016 were covered by a later ash and scoria layer, which resulted from the Episode 2 Strombolian eruptions.

4.4 Research Vessel Observations After Episode 4

Episode 4 caused the most significant change in the geology of the new island. We surveyed the topography and deposits of the island and obtained samples from representative locations using a drone in December 2020. Except for few locations on the southwest and northwest coasts, nearly the entire lava flow field had been covered by pyroclastic deposits. At the sea cliff, we observed a cross section of the stratified pyroclastic fallout tephra covering the lava flows effused during the early activity of Episode 4. In the north, the tephra deposit was more than 5-m thick (**Figure 5E**), reflecting the northward direction of the major tephra dispersal axis during the explosive phase, as observed by satellites. All the tephra layers were originated during the most intense explosive phase accompanying the lava-fountain activity and later phreatomagmatic explosions that occurred after June 2020.

4.5 Chemical Composition of Eruptive Products and Magma Reservoir Conditions

4.5.1 Chemical Characterization of the Eruptive Products

On the basis of the microscope observations, all the products from Episode 1–3 include phenocrysts of plagioclase, clinopyroxene (augite, pigeonite only for the phenocryst rims and groundmass), orthopyroxene, and Fe-Ti oxides less than 1 mm in length, while products of the Episode 4 exclude orthopyroxene and include olivine phenocrysts (**Figure 6**). Some of these phenocrysts appear as aggregates (glomeroporphyroclasts). The total phenocryst content was less than 10 vol% for all the products. The whole rock chemical compositions of the Episode 1–3 products are 59.2–59.9 wt% SiO_2, 2.3–2.5 wt% MgO, and 5.2–5.5 wt% $Na_2O + K_2O$ (**Figure 7**, **Table 2**, **Supplementary Table 1**) and are classified as andesite (Le Bas et al., 1986). Compared with rocks effused before 2013 (Ossaka et al., 1974; Ossaka, 1975, Umino and Nakano, 2007; Sano et al., 2016), all the products have a chemical composition intermediate between that of the products of the 1973–1974 eruptions with 58.6–59.1 wt% SiO_2 and that of the prehistoric (prior to 1702) lava with 60.1–60.8 wt% SiO_2. Conversely, the products of the late Episode 4 have 54.8–55.1 wt% SiO_2, 3.9–4.0 wt% MgO, and 4.0–4.1 wt% $Na_2O + K_2O$ (**Figure 7**) and are classified as basaltic andesite. Such chemical characteristics of magma with lower SiO_2 (higher MgO, **Table 2**) content in the whole rock chemical composition have never been reported before for on-land products from the recent Nishinoshima eruptions, although there is a report of the presence of mafic rocks with unknown ages in the submarine flank and satellite cones of the Nishinoshima (Tamura et al., 2018). Furthermore, the chemical composition trend observed throughout Episodes 1–3, which becomes more mafic with time, does not project to the whole rock compositions observed for Episode 4 (**Figure 7**).

The time-series whole rock chemical compositions of the erupted magma plot along a single trend, where the SiO_2 content gradually decreased with time before dramatically changing before or during Episode 4 (**Figures 4**, **8**). The tendencies of the other elements are similar (**Figure 8**). A few samples obtained by remotely controlled aerial vehicles, with unknown eruption dates, do not plot in this trend; however, most of lava samples fall along this trend and are temporally correlated. Furthermore, incompatible element concentration ratios, such as K_2O/TiO_2, Zr/Y, and Ba/Zr, in the whole rock composition mostly did not change after Episode 3 but increased before or during Episode 4 (**Figure 8**).

Throughout Episodes 1–3, the scoria and ash groundmass consist of glass that is black or brown in color with microlites of plagioclase and pigeonite. The Episode 4 groundmass has similar characteristics to those of Episodes 1–3, except for the absence of pigeonite microlites. The chemical

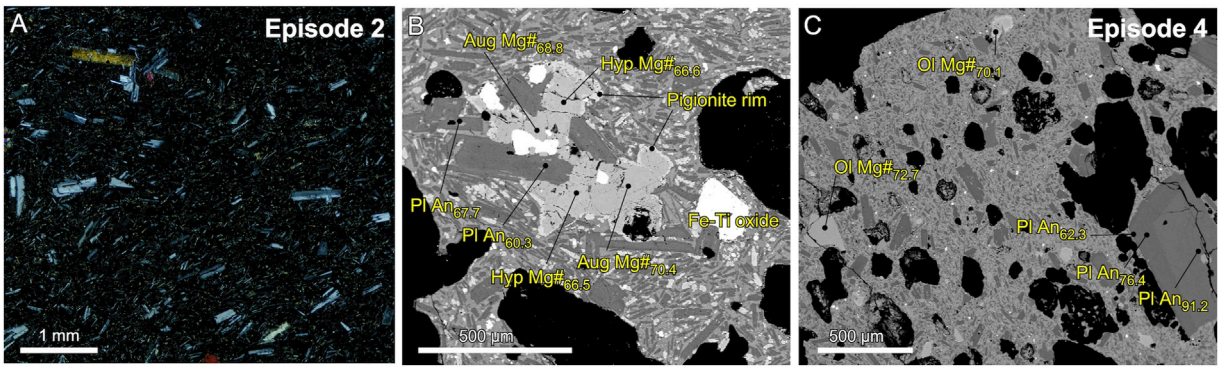

FIGURE 6 | (A) Microphotograph of lava from the 2017 eruption (Episode 2); **(B)** scanning electron microprobe image of a typical early-episode glomeroporphyroclast in scoria lapilli; and **(C)** scanning electron micro-image of scoria lapilli from the 2020 Nishinoshima eruption. Aug, Augite; Hyp, Hypersthene; Pl, Plagioclase; and Ol, Olivine are indicated with major chemical compositions.

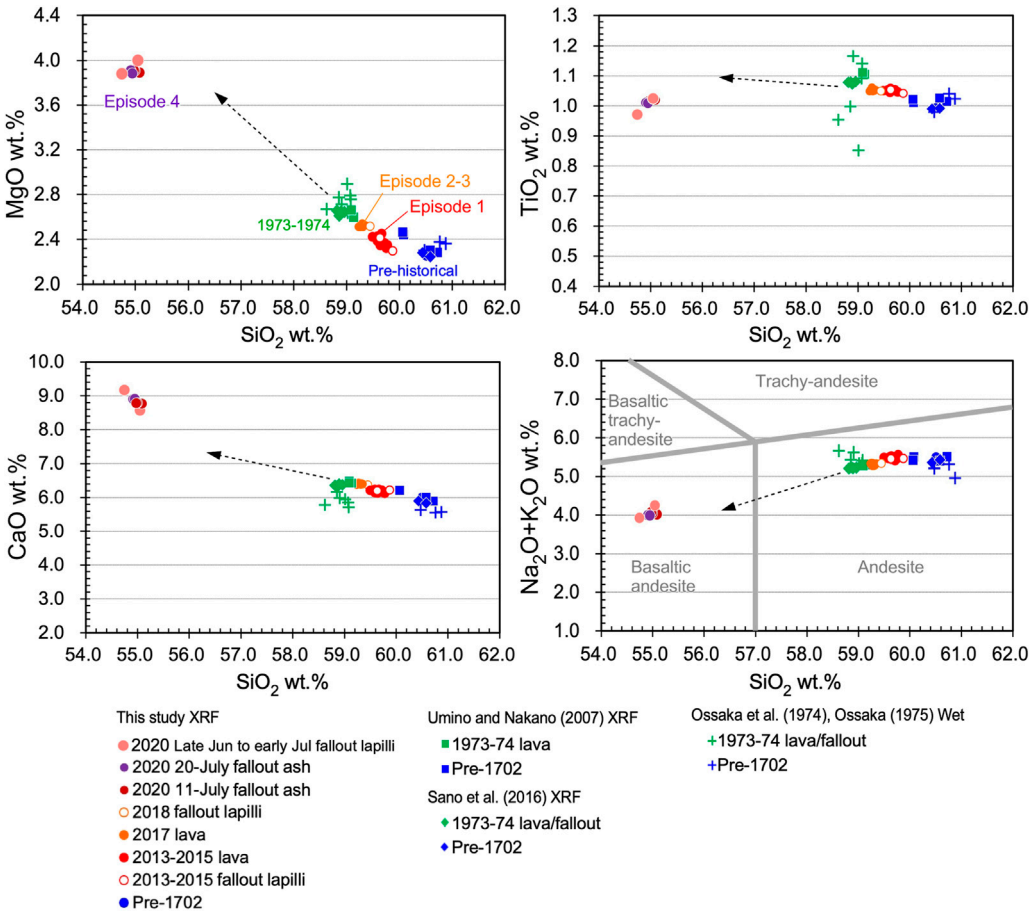

FIGURE 7 | Whole rock major element chemical compositions for representative samples from different Nishinoshima eruptions. Classification from Le Bas et al. (1986). Arrows indicate the direction of the mixing endmember component for the Episode 1–3 magma, which is slightly different from that of Episode 4.

composition of the groundmass glass of each sample varies with crystallinity; however, there is also a variation between Episode 1–3 and 4 that cannot be explained by the degree of crystallization (**Figure 9**). Most of the Episode 1–3 products have 62–69 wt% SiO_2; however, the Episode 4 products have 56–60 wt% SiO_2 (**Supplementary Table 2**). A compositional gap therefore exists in the groundmass glass, as in the whole rock chemical compositions.

TABLE 2 | Whole rock major and trace element compositions for representative samples from Nishinoshima volcano.

Sample name	NSN19090302a	NSN161020-07	NSN161020-10a	NSN19090303a	NSN19090509a	NSN201906	201223 HX01	201223 HX03-01
	Episode 1	Episode 1	Episode 1	Episode 2	Episode 2	Episode 3	Episode 4	Episode 4
Eruption date (from)	2013/11/22	2014/10/16	2015/3/23	2017/4/17	2017/5/1	2018/7/12	2020/6/1	2020/6/1
(to)	2014/3/1	2014/12/4	2015/3/25	2017/4/28	2017/6/5	2018/7/18	2020/6/30	2020/6/30
Major element (wt%)								
SiO_2	59.88	59.62	59.58	59.31	59.30	59.45	54.74	55.05
TiO_2	1.04	1.05	1.06	1.06	1.05	1.05	0.97	1.02
Al_2O_3	15.32	15.42	15.42	15.46	15.48	15.45	16.76	15.97
tFeO	9.15	9.34	9.30	9.46	9.46	9.34	10.17	10.75
MnO	0.21	0.21	0.21	0.21	0.21	0.21	0.20	0.21
MgO	2.30	2.39	2.43	2.51	2.54	2.51	3.88	4.00
CaO	6.22	6.17	6.25	6.39	6.41	6.38	9.17	8.57
Na_2O	4.21	4.30	4.26	4.17	4.13	4.17	3.13	3.47
K_2O	1.25	1.21	1.22	1.16	1.14	1.16	0.79	0.78
P_2O_5	0.43	0.29	0.29	0.28	0.28	0.28	0.18	0.19
FeO/MgO	3.98	3.90	3.83	3.77	3.72	3.72	2.62	2.69
Total	100.00	100.00	100.00	100.00	100.00	100.00	100.00	100.00
Trace element (ppm)								
Sc	19	20	19	20	19	20	32	33
V	161	166	172	183	186	181	317	335
Co	19	20	20	21	22	20	28	32
Cu	133	140	135	141	119	122	160	152
Zn	105	103	102	99	104	100	87	91
Ga	16	17	18	18	18	17	17	16
Rb	20	20	22	18	17	19	12	12
Y	39	39	39	37	37	37	28	30
Sr	226	226	227	224	225	224	241	232
Zr	116	119	119	111	111	113	72	75
Nb	3	3	3	3	3	4	2	2
Ba	291	290	281	273	279	264	190	188
Pb	4	3	3	3	1	3	2	2
La	9	5	4	10	7	9	3	5
Ce	28	29	26	22	28	24	10	16

The plagioclase phenocrysts (0.1–0.2-mm long axis) were divided into two types: Ca-rich cores with An_{80-95} (type 1) [An, anorthite content: 100 × Ca/(Ca + Na)] and Ca-poor cores with An_{55-80} (type 2) (**Figure 10**). Type 2 was further divided into type 2A, which has sodic rims with $An_{<60}$, and type 2B, which does not have sodic rims (**Figure 10**). The groundmass plagioclase has nearly the same composition ($An_{<60}$) as the type 2A rims. Type 2 is often characterized by multiple zoning and appears to be one of the glomeroporphyroclast phases. All of these types of plagioclase phenocrysts are observed throughout the recent eruptions; however, their ratio changes with the eruptive episode (**Figure 10**): for Episodes 1 and 2, type 2A is dominant and a small amount of types 1 and 2B appears; for Episode 3, type 2A decreases while type 1 and 2B slightly increase; and for Episode 4, types 1 and 2B become dominant and there is a decreased amount of type 2A.

The clinopyroxene and orthopyroxene phenocrysts of Episodes 1–3 are divided into two types: 1) a small amount of isolated microphenocrysts and 2) one of the glomeroporphyroclast phases, which is the more abundant and coexists with type 2A plagioclase and Fe-Ti oxides (**Figure 6B**). The microphenocrysts are finer in size (0.1–0.2-mm long axis) than the glomeroporphyroclast phases, while the glomeroporphyroclast phases are coarser (0.5–1-mm long axis). The chemical composition of the clinopyroxene (augite) is $Mg\#_{63-73}$ [Mg#: 100 × Mg/(Fe + Mg)] with a smaller Mg# for the microphenocrysts ($Mg\#_{63-68}$) and a higher Mg# for the glomeroporphyroclasts ($Mg\#_{66-72}$), many of which have pigeonite rims with $Mg\#_{54-60}$ (**Figure 10**). During Episode 4, more Mg-rich augite (average ~$Mg\#_{72}$) appeared and pigeonite disappeared. The chemical composition of the orthopyroxene is $Mg\#_{62-71}$ with a smaller Mg# value for the microphenocrysts ($Mg\#_{62-66}$) and a higher Mg# for the glomeroporphyroclasts ($Mg\#_{65-71}$). Some orthopyroxenes also have a pigeonite rim with $Mg\#_{54-60}$. During Episode 4, the orthopyroxene phenocrysts disappeared (**Figure 10**).

Olivine phenocrysts (0.1–0.4-mm long axis) only appear in the Episode 4 products. The most abundant chemical composition of olivine is $Mg\#_{68-70}$; however, higher $Mg\#_{>80}$ olivine also appears (**Figure 10**). Some of the olivines are characterized by normal zoning and have a rim with lower Mg#.

Melt inclusions (MIs) in plagioclase, pyroxene, and olivine phenocrysts also display a compositional gap as in the whole rock

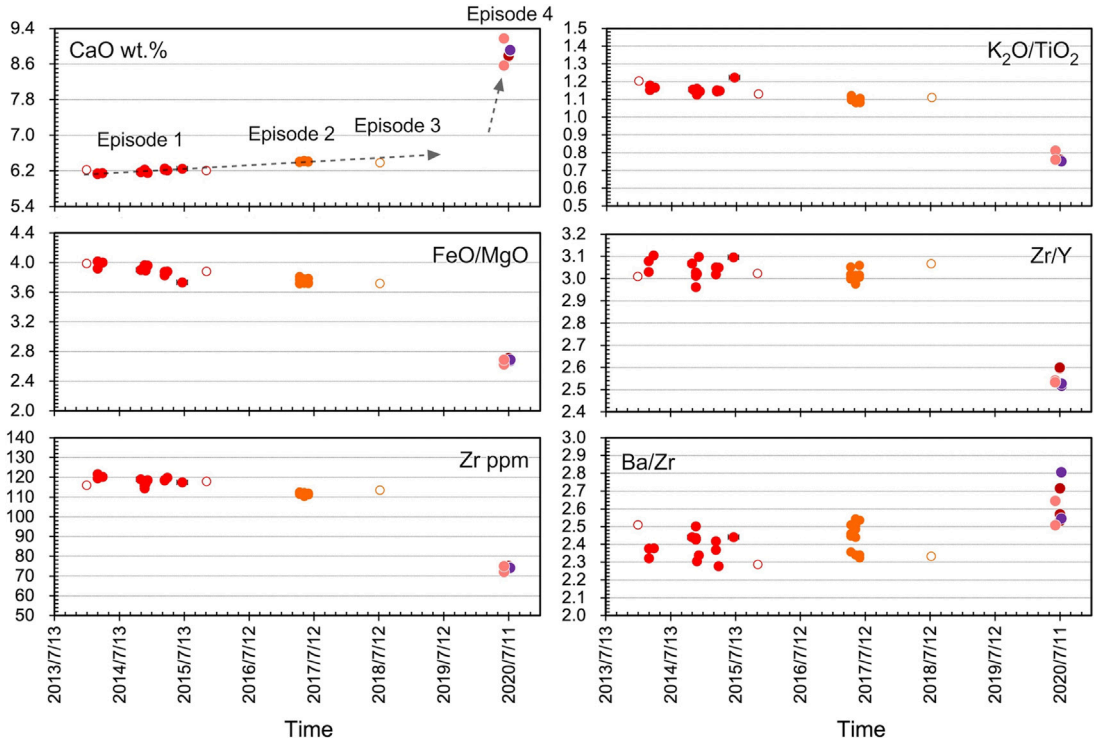

FIGURE 8 | Temporal variation in the whole rock major and trace element chemical compositions and their ratios throughout the recent Nishinoshima eruptive episodes.

and groundmass glass chemical compositions. Most of the Episode 1–3 MIs have 60–68 wt% SiO_2; however, the Episode 4 MIs have 55–59 wt% SiO_2, making them slightly more mafic than the groundmass glass (**Figure 11**, **Supplementary Table 3**). Some MIs in the Episode 4 olivine have undifferentiated features. The most mafic MI (46.8 wt% SiO_2 and 11.2 wt% MgO) was used to estimate the crystallization process of the mafic melts, as shown in **Figure 11**.

4.5.2 Magma Storage Conditions

The variation in the geochemical data suggest that the recent Nishinoshima eruption was linked to multiple magma reservoirs. In this section, magma storage conditions are estimated based on the chemical compositions of phenocrysts, groundmass glass, and MIs.

For Episode 1–3 magma with higher SiO_2 content, the magma temperature and water content were investigated using the MELTS program (Gualda et al., 2012) for a pressure range 0.5–1.5 kb. The MELTS fractionation models for the melt with a whole rock composition in Episode 1–3 best fit the compositional variation of MIs and groundmass in Episode 1–3 using a temperature and water content of ~1,050°C and 0.5–1.5 wt%, respectively (Maeno et al., 2018) (thick arrow A in the SiO_2-TiO_2 field in **Figure 11**). Furthermore, the MI water content in the type 2 plagioclase (abundant in Episodes 1–3 products) was estimated to be 1.5–2.0 wt% *via* direct measurements with Fourier-transform infrared spectroscopy (FTIR) (Maeno et al., 2018). The saturation pressure for these water contents corresponds to a depth of ~1.5–2 km. Using a pyroxene-melt geothermometer (Putirka, 2008) and the water content (by FTIR), the magma temperature of individual clinopyroxene phenocrysts was estimated to be ~1,050°C. This result is consistent with that of Maeno et al. (2016), where a similar temperature (1,050–1,090°C) was estimated for the crystallization temperature of groundmass crystals in volcanic ash from Episode 1, based on chemical compositions of the clinopyroxene (pigeonite) and groundmass glass. Conversely, the pyroxene phenocrysts in the glomeroporphyroclasts showed a lower magma temperature, ~970°C, using a two-pyroxene thermometer (Putirka, 2008). This result suggests different crystallization temperatures for the two types of pyroxene phenocrysts. This temperature is consistent with the results of Sano et al. (2016), who estimated a magma temperature of 970–990°C using a two-pyroxene thermometer for the products of Episode 1; this temperature is thought to correspond to the conditions of the highly crystallized part of the shallow magma reservoir. Type 2A plagioclase is also thought to form in this shallow reservoir.

However, the linear chemical trend that formed progressively from Episodes 1 to 3 (**Figures 7**, **11**) and the multimodal composition of the plagioclase and clinopyroxene phenocrysts and its change toward more mafic composition with time (**Figure 10**) suggest that there

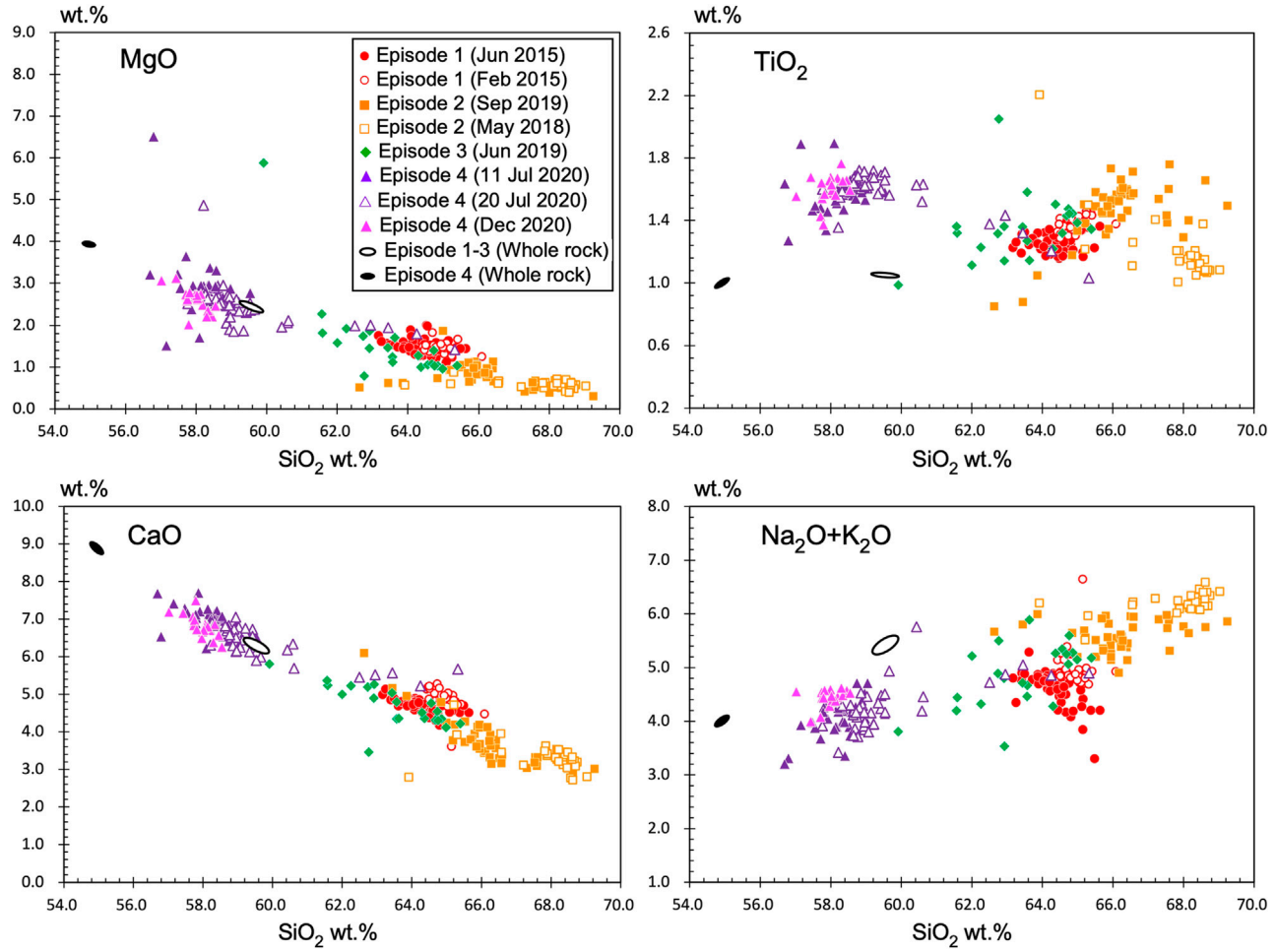

FIGURE 9 | Major element chemical compositions of the groundmass glass of representative samples from the recent Nishinoshima eruptions. Whole rock chemical compositions are also indicated. Dates in parentheses indicate those sampled.

is an endmember component that mixed with the silicic magma in the shallow reservoir. This endmember component is slightly different from the whole rock composition of the Episode 4 magma (**Figure 7**) but is assumed to be a magma having the average composition of the major Episode 4 MI (green field in **Figure 11**). The Episode 4 groundmass glass compositions can be explained by the fractionation of magma with a melt composition that is the same as the Episode 1–3 endmember component (thick arrow B in **Figure 11**). In this case, a similar magma temperature and water content to those of the Episode 1–3 magma (1,050–1,100°C and 0.5–1.5 wt% H_2O) are estimated, while the pressure is not constrained.

The Episode 4 magma also contains high-Mg# olivine (>80) with MIs more mafic than the whole rock chemical composition (**Figures 10**, **11**). Because this high-Mg# olivine cannot be equilibrated with most of the Episode 4 melt, a more mafic magma must have been included with the mixture. The MI compositional variation, which is more mafic than the Episode 4 whole rock composition, also indicates the mixture of a range of mafic melts.

As an attempt to explain these geochemical features, assuming the most mafic MI (46.8 wt% SiO_2 and 11.2 wt% MgO), which is hosted in olivine with $Fo_{87.6}$ as the undifferentiated basaltic magma, we investigated if the observed compositional variation of the plagioclase and olivine phenocryst cores could be explained (**Figures 11**, **12**). In **Figure 11**, the equilibrium and fractional crystallization paths (liquid lines of descent) calculated using the MELTS program (Smith and Asimow, 2005; Gualda et al., 2012) for different initial conditions (water content and pressure) buffered by FMQ are shown. In this calculation, olivine with Fo > 85 appears at temperatures of > 1,170°C for 1 wt% H_2O and > 1,120°C for 3 wt% H_2O (**Figure 12**). Olivine with Fo~70, which is the compositional majority in Episode 4, is explained by fractional crystallization at a temperature 1,050–1,080°C at 1–3 kbar in the case of 1 wt% H_2O. If the water content increases to 3 wt%, a lower pressure of 1–2 kbar is acceptable to form Fo~70 olivine. High-An (>90) plagioclase can crystallize at >1,150°C for 1 wt% H_2O and at 1,010–1,140°C for 2–3 wt% H_2O; however, higher An plagioclase can more easily crystallize

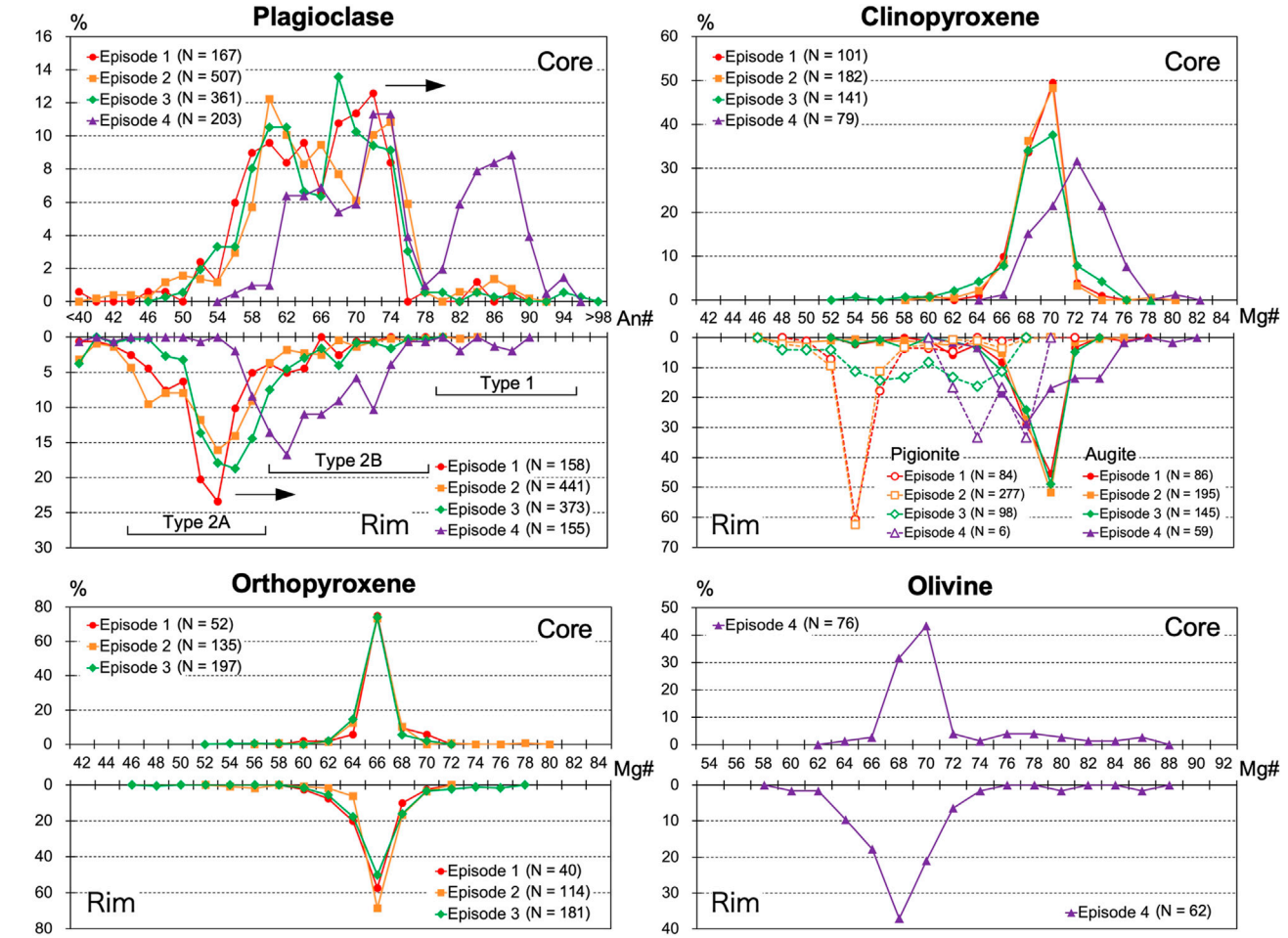

FIGURE 10 | Variation in the chemical composition of the phenocryst core and rim for Episodes 1–4. Black arrows in the plagioclase show the direction of the temporal change.

at lower pressures (1–2 kbar) and higher water contents: An_{95}, which is the highest observed, appears at 1,090–1,110°C and 1–2 kbar for 3 wt% H_2O. Type 1 ($An_{80\text{-}90}$ core) plagioclase can be explained by a temperature range of 1,000–1,100°C (**Figure 12**).

At this stage, we have no further constraints; however, we can infer that plausible conditions for the deep reservoir are 1,050–1,110°C and 1–2 kbar, which can explain major olivine (Fo~70) and plagioclase (type 1) compositions in Episode 4. Furthermore, the water content 2–3 wt% H_2O is required to explain the presence of high-An plagioclase in Episode 4. Therefore, it is possible that the water content increased in the deep reservoir before or during Episode 4. The absence of orthopyroxene in Episode 4 can be explained by the crystallization process assumed here because it first appears at temperatures of <1,050°C under conditions with ≤3 wt% H_2O and pressures of ≤2 kbar, while clinopyroxene appears at >1,100°C. This phase relationship is consistent with the observations.

The equilibrium or fractional crystallization paths calculated using the most mafic MI can produce a range of chemical compositions that might correspond to the mafic endmember melt (**Figure 11**), where the observed high-Mg# olivine and high-An plagioclase are survival crystals in the most mafic melt (**Figure 12**). Mixing of the differentiating mafic melt and the silicic melt (with the groundmass glass composition of Episode 4) may explain the MI compositional variation during Episode 4. It may also control the whole rock chemical composition of the Episode 4 magma, which is slightly different from the endmember component in Episodes 1–3. Some mafic MIs (outliers with 51 wt% SiO_2) cannot be explained by this mixing process, and it is thought that another mafic melt was also involved.

5 DISCUSSION

5.1 Variation in the Eruptive Style

A major characteristic of the Nishinoshima eruptive activity is that the growth of the island was largely dominated by lava effusion but also pyroclastic cone formation, which indicate the

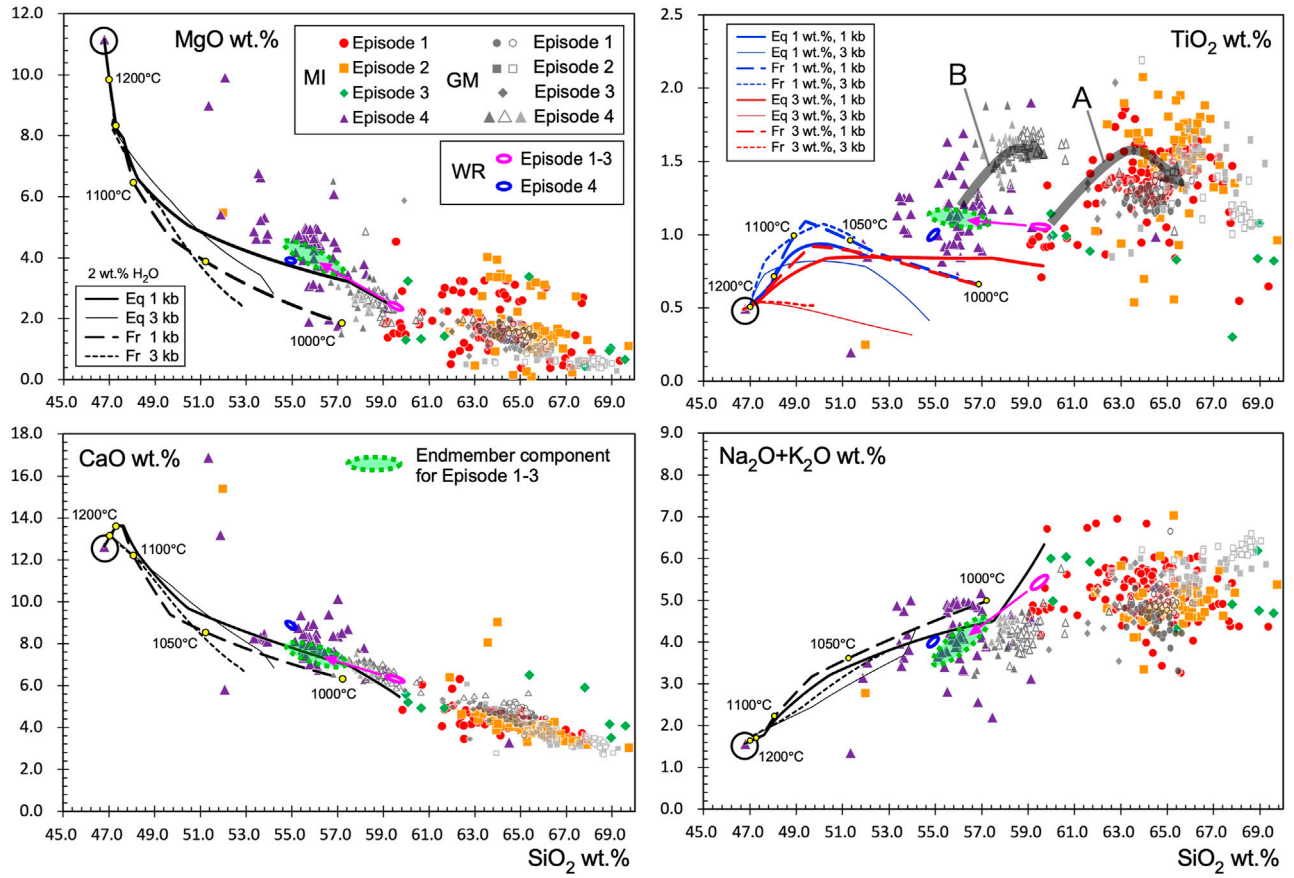

FIGURE 11 | Major element chemical compositions of melt inclusions (MIs, olivine-hosted and plagioclase-hosted) for representative samples from the recent Nishinoshima eruptions (colored symbols), plotted with the groundmass glass (GM) and whole rock (WR) chemical compositions. Symbols for GM are the same as in **Figure 9**, but grayscale is used; dark and light gray filled triangles: Jul 11, 2020 and Dec 2020, respectively. Arrows from the WR (the same as in **Figure 7**) indicate the direction of mixing of the endmember compositions (green area) in Episodes 1–3. Equilibrium (Eq) and fractional (Fr) crystallization paths (liquid lines of descent, LLDs) for the basaltic MI in olivine (denoted by the large circle) calculated using the MELTS program for different initial conditions (water content and pressure) buffered by FMQ are shown (black lines for MgO, CaO, and $Na_2O + K_2O$ and colored lines for TiO_2). For the black lines, only cases with 2 wt% H_2O are shown. Yellow dots indicate the temperatures every 50°C for 1 kbar and 2 wt% H_2O. The thick gray arrows A and B in TiO_2 show the approximate LLDs for water contents of <1.5 wt%, assuming the initial melt compositions of Episodes 1–3 and 4, respectively.

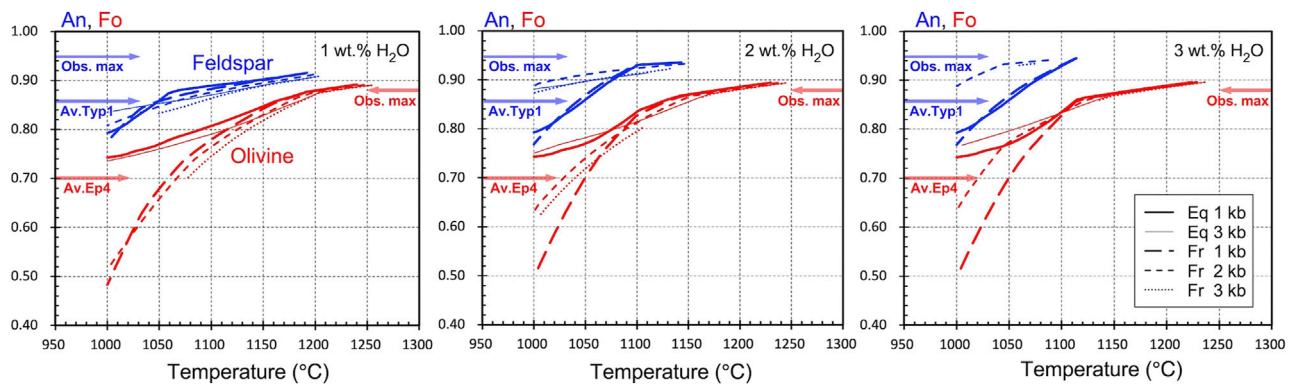

FIGURE 12 | Relationships between the anorthite (An) or forsterite (Fo) contents of feldspar and olivine, respectively, and the temperature down to 1,000°C for different initial water contents calculated using the MELTS program assuming equilibrium (Eq) and fractional (Fr) crystallization of the most mafic olivine-hosted MI in Episode 4 (the same as that circled in **Figure 11**). For feldspar, the observed maximum An (obs. max: ~0.95) and averaged An of type 1 plagioclase (av. typ 1: ~0.85) are indicated. For olivine, the observed maximum Fo (obs. max: ~0.88) and averaged Fo of Episode 4 olivine (av. Ep4: ~0.70) is indicated.

hybrid activity by effusive and explosive eruptions (**Figures 2**, **3**). The lava flows branched repeatedly and formed a large number of small and large lava lobes, namely, compound lava flows. Compound lava flows are generally observed in low-viscosity basaltic lava (Walker, 1971; Kilburn and Lopes, 1988; Calvari et al., 2002). The intermittent explosive activity characterized by Strombolian eruptions (from Episode 1 to early Episode 4) also suggests low-viscosity flows. In low-viscosity magma, efficient gas–melt segregation can occur, which may cause moderately explosive behavior due to the expansion of the gas-rich part of the magma (e.g., Edmonds, 2008; Taddeucci et al., 2013). Conversely, degassed magma, which has high density, may move laterally and yield lava flows if the conduit pressure overcomes the strength of the scoria cone. This type of hybrid activity has been recorded for pyroclastic cone formation by mafic magmas (Valentine et al., 2005; Pioli et al., 2008; Rowland et al., 2009).

Looking only at the whole rock chemical composition, andesite magma with 59–60 wt% SiO_2 may cause explosive activity or viscous lava flows/domes than more mafic compositions, as observed in many andesitic arc volcanoes (e.g., Murphey et al., 2000; Suzuki et al., 2013); however, this is not the case for Nishinoshima. This is because the Nishionoshima magma has a relatively high temperature (1,050–1,100°C) and lower phenocryst content (< 10 vol.%). These conditions can cause a minimum estimate of viscosity of 10^4 Pa s (Maeno et al., 2016) and may cause eruptive behavior similar to basaltic volcanism. Maeno et al. (2016) proposed that the lava flow dynamics of Nishinoshima is primarily controlled by the low magma viscosity, low magma discharge rate, and a higher cooling efficiency compared with terrestrial lava flows based on a theoretical consideration by Blake and Bruno (2000). In fact, the chemical composition of the magma gradually changed with time, becoming increasingly mafic. However, before Episode 4, the change in SiO_2 content was only ~1 wt %, corresponding to only a ~0.2 log unit in viscosity based on the model of Giordano et al. (2008). Such a change would not be able to cause the significant observed changes in the physical properties of the magma, eruptive style, and lava emplacement processes. Our land surveys and remote observations also suggest that there are no differences between Episodes 1 and 2 in the external/internal structures of their lava flows and that they reflect their emplacement processes.

The change in the chemical composition of the magma in Episode 4 might have significantly affected the eruptive style. In June–July 2020, there was a dramatic change in the style from lava flow-dominated to pyroclast-dominated, causing the cone to rapidly grow to a height of 250 m and a diameter of 570 m within a single month. Before 2020, the pyroclastic cone was only <10% of the island volume; however, after June 2020, the volume ratio of the cone increased to 60%. The entire island was also covered by thick pyroclastic fallout deposits. The eruptive style of this explosive type was interpreted to be violent Strombolian (Yanagisawa et al., 2020) as in geological and historical records of explosive basaltic eruptions (Arrighi et al., 2001; Valentine et al., 2007; Pioli et al., 2008; Di Traglia et al., 2009), and suggests that magma fragmentation was more efficient and caused the significant morphological change of the island.

The explosivity of low-viscosity magma is controlled by the degree of gas–melt segregation and the magma ascent velocity (e.g., Parfitt, 2004; Edmonds, 2008; Gonnermann and Manga, 2013; James et al., 2013; Taddeucci et al., 2013). Lava fountains with vigorous ash plumes, as observed during Episode 4, are generally thought to represent the closed-system degassing end member at high magma ascent rates. During the Episode 4, the magma discharge rate (ascent rate if conduit radius not changed) higher than those of the previous activities was estimated from the thermal anomaly intensity and optical satellite observations (**Figure 4**)[1]. Thus, the transition of eruption style from intermittent Strombolian to more continuous and intense lava fountaining is thought to have been caused by the increase of magma ascent rates. The gas–melt segregation efficiency might be also affected by the melt viscosity and its change during ascent, such as *via* microlite crystallization (Polacci et al., 2006; Houghton and Gonnermann, 2008; Cimarelli et al., 2011), but the eruption style and explosivity can be primarily controlled by elementary factors such as the volatile content in the reservoir (e.g., Sides et al., 2014). The higher initial volatile content can contribute to make higher exit velocity at vent, thus resulting in higher fountains (e.g., Wilson and Head, 1981; Parfitt, 2004).

The dramatic change in the chemical composition of the magma in the later phase of Episode 4 suggests that there was a large amount of mafic magma recharge from the deeper part of the magma system (**Figure 13**). This is consistent with the apparent increase in the sulfur component of the satellite-observed volcanic gas, indicating the recharge of volatile-rich mafic magma[1]. Our geochemical monitoring data also showed the possibility of increased volatile content in the magma, as indicated by the increase in higher-An (type 1, An > 90) plagioclase (**Figures 10**, **12**). These observational and geochemical data suggest that the major factors in the explosivity increase observed during Episode 4 were the change in the volatile (vapor phase) content in the magma-storage region, the increase in the mass discharge rate, or both, resulted from mafic magma recharge in depth. More direct evidence for the transition of eruption style and its causes is required to provide better constraints. They might be recorded in micro-scale rock textures or volatile species and their concentrations in crystal and melt phases.

During the period just before the cessation of each eruptive episode, Vulcanian-type explosions were observed. This change in the eruptive style is a common characteristic of Nishinoshima magma. Regardless of the chemical compositions of the erupting magma, the decrease in the average rates of magma ascent may allow an increase in the magma viscosity in shallow conduits because of slow magma ascent, or a longer residence time, which causes more extensive degassing and crystallization. This eventually inhibits two-phase flow and causes the formation of an impermeable plug on top of the conduit, decreasing degassing and increasing the overpressure in the shallow magma, resulting in an intense explosion (Sparks, 1997; Stix et al., 1997). This type of Vulcanian activity caused by mafic magma was also observed in the 1943–1952 eruption of the Paricutin volcano, Mexico (Pioli et al., 2008).

The change in the eruptive style from Strombolian to Vulcanian was observed in Episodes 1 and 2. During this

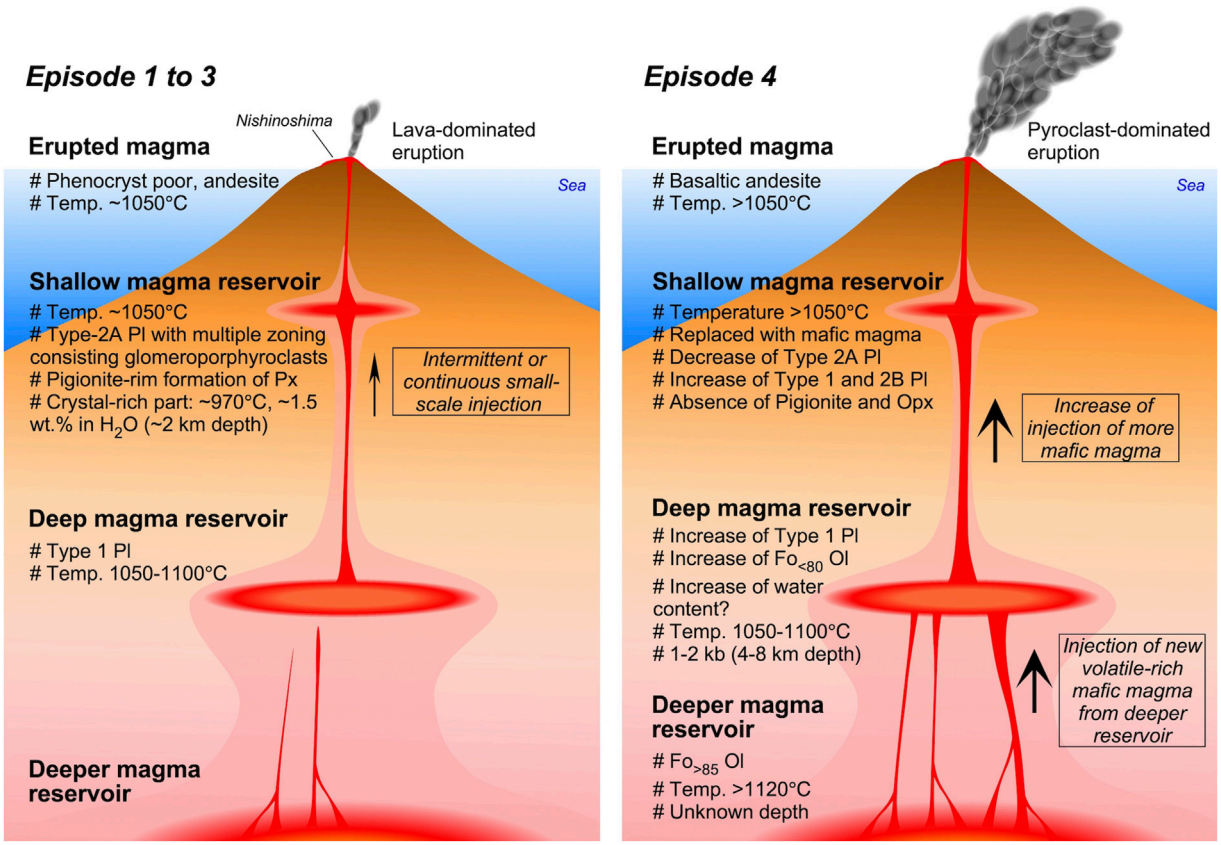

FIGURE 13 | Schematic diagram of the magma reservoirs and feeding system thought to have developed beneath Nishinoshima volcano.

period, the summit crater was enlarged and the height of the cone slightly decreased (**Figures 3**, **4**) as a result of the expulsion of the summit rocks by intense explosions. For Episodes 3 and 4, whether Vulcanian-type explosions occurred is unknown.

5.2 Implication for the Magma Feeding System

The erupted volume gradually decreased during the three episodes from 2013 to 2018. Before 2019, we interpreted this observation as indicating that the recent Nishinoshima activity was headed toward cessation in the long term as a result of the decreasing overpressure in the magma reservoir. However, the erupted magma shows evidence of an increased contribution of magma mixing; for example, the whole rock chemical compositions have become more mafic in the later activity and there was an increase in type 1 plagioclase with high-An cores. In just Episode 1, the mafic component in the whole rock major element composition gradually increased. These data indicate that the ratio of the mafic component increased as the result of multiple and intermittent mafic magma recharge from a deep reservoir (4–8 km) into a shallow magma reservoir (1.5–2 km) or a decrease in the volume of the silicic component in the shallow magma reservoir (**Figure 13**). Baba et al. (2020) estimated the demagnetization source and pressure source depths to be 2.6 km below sea level (b.s.l.) and 6.6 km b.s.l., respectively, using ocean bottom electromagnetometers installed offshore the island from 2016 to 2017. The depths of the deep and shallow reservoirs may be related to these magnetic and pressure sources, although there is a little discrepancy for the shallow source.

The onset of Episode 4 in December 2019, with more explosive eruptions and a higher magma discharge rate, and the change of magma from andesite to basaltic andesite suggest that the recent activity was not actually declining but that there was a large mafic magma recharge. In addition to a large amount of volatile release during the most intense phase of Episode 4, previously unrecognized olivine phenocrysts have been incorporated into the magma and incompatible element concentration ratios, such as Zr/Y, in the whole rock compositions have changed. Therefore, we suggest that a new undifferentiated, volatile-rich magma, different from the mafic magma that was involved in the earlier eruptive episodes, ascended from an additional source (deeper than 8 km) and dramatically changed the eruptive style to be more explosive in Episode 4.

The observations are difficult to explain using only the magma reservoirs that caused Episodes 1–3. Undifferentiated magma might have ascended from depth, or the discharge of a large volume of magma from the shallow magma reservoir might have triggered the movement, redistribution and ascent of deeper magma. If we assume that the endmember mafic magma in

Episode 4 exists on the calculated LLDs and that the temperature is 1,050–1,100°C (**Figure 11**), the weight ratio of the mixed endmember mafic magma will be approximately 20–30%. This probably caused a significant change in magma reservoir condition, hence the change in eruptive behavior, although the relationship between the volume of mafic magma involved and the eruption style and magnitude may not be straightforward. Geochemical monitoring data suggests that the recent eruptive activity and growth of Nishinoshima have been fueled by intermittent or continuous mixing in the shallow reservoir and more episodic and large-scale magma recharge from deeper parts of the magma-feeding system (**Figure 13**). The temperatures of the shallow and deep reservoirs are not significantly different, meaning that deep magma can be supplied to shallow levels with limited cooling. Therefore, it is thought that deeper magma injection significantly controlled the eruptive activity during Episode 4.

5.3 Morphological Development and Growth of the Island

In the effusive phases by low-viscosity andesitic magma, lava was supplied from the center of the island with some fluctuations in the discharge rate and flowed along topographic lows. It formed both small and large lava lobes, increasing the area of the lava field. This process formed the complicated irregular morphology of Nishinoshima. This was observed particularly in the middle of Episode 1, Episode 2, and the earlier phase of Episode 4 and it is thought to reflect the lava flow dynamics, which is primarily controlled by the lower magma discharge rate (Maeno et al., 2016). Low-viscosity lava basically spreads horizontally and enlarges the area of effusive products, following its gravity flow nature (e.g., Huppert et al., 1982; Griffiths, 2000). The final morphology of the lava flows is controlled by the viscosity, cooling rate, and effusion rate (Griffiths and Fink, 1992; Blake and Bruno, 2000; Anderson et al., 2005; Harris et al., 2007), and lava flows fundamentally contribute to the lateral growth of the volcanic edifice.

The contribution of lava flows to island growth and morphological characteristics on Nishinoshima is observed at other volcanoes where silicic lava flows with multiple lobes, inflation clefts, and breakouts spread onto the shallow seafloor, such as andesite lavas from the Sakurajima volcano, Japan (Omori, 1916), andesite lavas from the Anak Krakatau volcano, Indonesia (Sutawidjaja, 2006), and dacite lavas from the Nea Kameni volcano, Greece (Pyle and Elliot, 2006). As Maeno et al. (2016) noted, the development of a solid crust at the lava flow margins may be pronounced in eruptions in marine and lacustrine settings and may be an enhancing factor in the emplacement processes of lava flows with multiple lobes.

When lava flows enter water, a large amount of steam rises from the front of the lava flow (**Figure 2**). The flow front is rapidly cooled as it comes into contact with the seawater and is presumably brecciated, or auto-brecciated by the motion of the lava flow. The development of platy joints surrounding the massive interior of a lava lobe may reflect rapid cooling in a single lava lobe, as observed in lava flows contacting ice (e.g., Lescinsky and Sisson, 1998). Although the submarine parts of the lava flows are not exposed, the lava-fed delta may be composed of hyaloclastites that are continuously produced at the front and base of the flow. These flows are extending the foreshore, as described for exposed ancient basaltic and andesitic lava flow successions (e.g., Schneider, 2000; Smellie et al., 2013), and contribute to the formation of the foundation of the volcanic island.

In addition to lava effusion, pyroclastic eruptions also contributed to the morphological development. The formation process of a central cone at Nishinoshima can be divided into two stages: the cone-building by accumulation of the ballistically ejected clasts from coarse-grained Strombolian eruptions in early stages (Episode 1 to mid-Episode 4) and the later cone-building by deposition of fine-grained tephra from more explosive eruptions in mid-Episode 4. The growth rate of the later cone was much higher than that of the earlier one (**Figure 4**), reflecting higher depositional (or magma discharge) rate in the middle of Episode 4. The early cone continued to grow upward and outward with a combination of ballistic emplacement and grain avalanching. The latter cone may be explained by the rapid accumulation of fine-grained fallout deposits from the sustained, well-fragmented eruption column, which is significantly different from the early episode. The dramatic changes of eruption style, depositional process, and resulting morphological feature, similar to Nishinoshima, have been reported for Lathrop Wells volcano, southern Nevada, United States (Valentine et al., 2005), where the clear boundary of the two different depositional processes between the early Strombolian eruption and the later violent-Strombolian eruption was identified. Although Valentine et al. (2005) argued that the change of the eruption style might be caused by increase of effective viscosity due to microlite crystallization, this may not be only the mechanism for such an eruption. In Nishinoshima, geochemical characteristics of the magma feeding system and their change by the recharge of more mafic magma played an important role on the eruption transition and the morphological development of the volcanic edifice.

Pyroclastic eruptions will be one of the major contributing factors for the growth of the cone in Nishinoshima. However, if such eruptions occur in a very initial phase of the island formation and pyroclasts mainly shape the island without lava flow effusion, they are likely to be easily and quickly eroded by waves. In the recent Nishinoshima eruption, the situation in which primary loose pyroclastic fall/flow deposits form coast lines was not observed. Rather, the lava flows that can control lateral growth played the most important role on the formation of the foundation of the island. In fact, wave erosion was observed on some near-shore lava lobes, particularly during the calm periods between the eruptive episodes. However, resedimentation of pyroclastic materials by waves also occurred, resulting in the formation of new beaches. These secondary processes of erosion and resedimentation have reshaped the irregular outline of the island to be more rounded with time (**Figure 3**); however, they do not appear to have significantly changed the surface area of the island, at least in the recent years.

5.4 Comparison With Historical Examples

Historical records of failed and successful volcanic island formation are available. The 1952–1953 silicic eruption at Myojinsho in the Izu-Bonin arc, Japan, created a small lava (dome) island in shallow water; however, this island was destroyed by numerous explosion episodes and disappeared because of the lack of further lava effusion, thus failing in forming a volcanic island (Morimoto and Ossaka, 1955; Fiske et al., 1998). The 1986 eruption at Fukutoku Okanoba, 300 km south of Nishinoshima, created a small pyroclastic cone in shallow water as the result of Surtseyan-type eruptions of trachytic magma (Ossaka, 1991). However, the cone was easily eroded within 3 months and no island formed. The ephemeral Ferdinandea Island produced by the 1831 Surtseyan-type eruption in the Strait of Sicily, Italy (Cavallaro and Coltelli, 2019), was also one of examples of failed volcanic island formation. Conversely, in the 1934–1935 eruption at Showa Iwo-jima, silicic lava effusion resulted in a new volcanic island (300 m × 530 m) that has survived 80 years, although wave erosion has decreased the size of the island. The duration of this eruption was only half a year (October 1934–March 1935); however, lava effusion occurred continuously and its effusion rate reached values of the order of 10^5 m^3/day (Maeno and Taniguchi, 2006), the same order observed during the recent Nishinoshima eruptions. During the first 5 months of the 1973–1974 Nishinoshima eruption, submarine eruptions occurred, and their products buried the funnel-shaped crater to a depth of ~100 m and then formed a new island with Surtseyan and Strombolian eruptions with lava effusion (Aoki and Ossaka, 1974; Ossaka et al., 1974; Ossaka, 1991). The eruptions occurred at a similar location to the recent activity since 2013. For this previous Nishinoshima eruption, the discharge rate was estimated to be 1×10^5 m^3/day for the submarine stage during the first 5 months, then decreasing to $2–4 \times 10^4$ m^3/day in the following 11 months of island forming activity. The magma discharge rate during the submarine stage was comparable to that of the recent eruptions. However, multiple subaerial vents and scattered small pyroclastic cones (with maximum heights of ~52 m) formed, confining the lava effusion rates at each vent. Although the eruption created a new island with an area of ~0.25 km^2 and a pre-erosion height of ~50 m (total volume, $\sim 2.4 \times 10^7$ m^3), most of the pyroclast-dominated island was eroded and only small portions of the lava-dominated parts withstood erosion by 2013. This previous Nishinoshima eruption differs from the recent events, in which continuous lava effusion occurred from almost the same location throughout four eruptive episodes over 8 years, resulting in an area of 2.6 km^2 (~10 times larger than the previous area) and a height of ~250 m.

As seen in the Nishinoshima eruption and other historical submarine eruptions in the Japanese archipelago, one of the important factors controlling whether a volcanic island is created is the volume and effusion rate of the lava flows in shallow seas. Large volumes of unerodable lava relative to pyroclastic material contribute to the enlargement of the foundation of a volcanic island. The Episode 1 lava volume of the recent Nishinoshima eruptions reached more than 1×10^8 m^3, corresponding to an eruption magnitude (M: Pyle, 2013) of ~4.5. The average lava effusion rate was $\sim 2.0 \times 10^5$ m^3/day. The magnitude of this eruption was the largest in Japan since the 1991–1996 Unzen eruption (M ~ 4.7) in which 2.1×10^8 m^3 of dacite magma were effused with an average magma discharge rate on the order of $\sim 10^5$ m^3/day (Nakada et al., 1999). In the case of Nishinoshima, long-term but episodic magma discharge has resulted in voluminous lava flows and an extension of the island area. The average magma discharge rate, 2.0×10^5 m^3/day (2.3 m^3/s) of the recent Nishinoshima eruptions is similar to the discharge rate (2–5 m^3/s) during the later phase of the 1964 Surtsey eruption, although the discharge rate of the Surtsey eruption reached 20 m^3/s on average in the early effusive phase with relatively high-intensity activity (Thordarson and Sigmarsson, 2009). Comparing the magma discharge rates at Nishinoshima with those of other island-forming eruptions, it appears that long-lasting lava effusion with a discharge rate on the order of at least 10^4 m^3/day (annual average) to 10^5 m^3/day (monthly average) is required for the formation and long-term survival of a new volcanic island in shallow seas. Specifically, effusive lava flows contribute to increasing the area of the island and to form the solid foundation of the island. Conversely, the vertical growth rate of an island may be controlled by tephra deposition, including pyroclastic cone formation. Explosive activity contributes to increasing the height of a volcano *via* pyroclastic deposits. This order of eruptive products from lava flows to pyroclastic deposits may be essential for the efficient growth of a volcanic island. At the time of writing, there was an explosive eruption at Fukutoku Okanoba volcano in Japan from the shallow sea floor on August 13–15, 2021 (confirmed by Japan Coast Guard), that formed a new island consisting of pyroclastic deposits. This island remains after several months; it will be interesting to see whether this island formation fails or succeeds.

6 CONCLUSION

Here, we reported the detailed sequence of the recent Nishinoshima eruptive events based on long-term geological and geochemical monitoring since 2013 and discussed the formation and growth processes of the new volcanic island and the temporal changes in the magma chemistry. The Nishinoshima eruptive activity can be divided into four episodes. Over the eruptive episodes, the growth of the new volcanic island was sustained by the effusion of andesite lava flows into the shallow sea at a rate of the order of 10^5 m^3/day. The lava flows spread radially with numerous branches, resulting in compound lava flows. This constituted the primary contributor to the construction of the solid foundation of the island; however, deposition of pyroclastic materials also helped expanding the subaerial volcanic edifice. The duration of the eruptive episodes was initially 2 years (Episode 1) but shortened to a week by Episode 3, with decreasing eruptive volume with time. However, the latest episode (Episode 4, 8 months of

activity) was the most intense and the largest episode with a magma discharge rate on the order of 10^6 m^3/day. The size of the new island reached 2.5 km × 2.5 km (~4.4 km^2) with a volume of ~0.2 km^3 by 2020. The eruptive style dramatically changed during Episode 4 from lava-dominated to more explosive pyroclast-dominated, and the volume ratio of the pyroclastic cone increased from <10 to 60%. However, the temporal change in the geochemical characteristics indicates that more mafic magma was involved in the later episode and that the initial andesite magma with ~60 wt% SiO_2 changed to basaltic andesite magma with ~55 wt% SiO_2 in Episode 4. The eruptive behavior and geochemical data suggest that the recent Nishinoshima eruptions were fueled by the intermittent or continuous mixing of silicic and mafic magmas in a shallow reservoir (~2-km depth) and by a more episodic and large-scale magma supply from deeper reservoirs.

Some of the important factors controlling volcanic island formation and growth in shallow seas are the volume and effusion rate of the lava flows. A larger volume of unerodable lavas rather than pyroclastic deposits contributes to enlarging the solid foundation of a volcanic island, as observed in the case of the recent eruption of Nishinoshima volcano. Comparisons with several examples of island-forming eruptions indicate that long-lasting lava effusion with a discharge rate of the order of at least 10^4 m^3/day (annual average) to 10^5 m^3/day (monthly average) is required for the formation and growth of a new volcanic island with a diameter on km-scale that can survive against sea waves over the years.

The longer-term eruptive history of Nishinoshima is not well understood; however, because it is growing a large volcanic edifice, Nishinoshima may continue to be very active over a long time and may repeat eruptive activity, such as the effusion of large amounts of lava, as in the recent eruptions. Most of the volcanic edifice is underwater; therefore, it is unknown whether submarine eruptive activity had recently occurred other than at the summit. To capture a complete view of the recent eruptive activity, it is necessary to perform detailed survey of the changes in the seafloor topography and ejecta. Comprehensive analyses of the eruptive materials are also expected to provide a detailed image of the magma feeding system that caused the recent eruptions and the processes of magma ascent. Further geological and geochemical analysis, as well as geophysical data, is crucial to provide an overall understanding of the Nishinoshima volcano.

DATA AVAILABILITY STATEMENT

The original contributions presented in the study are included in the article/**Supplementary Material**, further inquiries can be directed to the corresponding author.

AUTHOR CONTRIBUTIONS

FM oversaw data collection and analysis and wrote the first draft of the manuscript. NH and AY conducted XRF and EPMA analyses, and FM and AY analyzed the dataset. TK, AY, and FM analyzed the satellite data. FM, TK, and SN (NIED) conducted aerial surveys, analyzed images, and made geological interpretations. FM, MY, and SN (AIST) conducted geological investigations and sampled rocks during the land surveys. YT, AT, and MT led the remote research vessel surveys and contributed to sampling and eruption chronology. All authors discussed the eruption process, cooperated in revisions, and approved this submission.

FUNDING

This research was supported by Grant-in-Aid for scientific research (No. 16H02221, 17H02987 and 21H01195) from the Ministry of Education, Culture, Sports, Science and Technology of Japan (MEXT), by Earthquake and Volcano Hazards Observation and Research Program of MEXT (ERI17) and by ERI JURP 2019-G-05 in Earthquake Research Institute, the University of Tokyo.

ACKNOWLEDGMENTS

We acknowledge the Nishinoshima comprehensive scientific research project led by the Ministry of the Environment Japan, specifically for the land surveys. Sampling of volcanic products from Nishinoshima were carried out in cooperation with shipboard scientists and technical personnel on multiple research vessels (*Kairei, Natsushima, Shinseimaru, Keifumaru, and Ryofumaru*). We also acknowledge the JCG and the GSI for providing their bathymetry data before the eruption and their topography data during the recent eruptions. Our aerial inspections were performed courtesy of Asahi Shimbun, Yomiuri Shimbun, and Mainichi Shimbun who kindly provided their aircrafts. We also thank the editors Joan Marti and Valerio Acocella and two reviewers for constructive comments and suggestions.

SUPPLEMENTARY MATERIAL

The Supplementary Material for this article can be found online at: https://www.frontiersin.org/articles/10.3389/feart.2021.773819/full#supplementary-material

REFERENCES

Anderson, S. W., McColley, S. M., Fink, J. H., and Hudson, R. K. (2005). "The Development of Fluid Instabilities and Preferred Pathways in Lava Flow Interiors: Insights from Analog Experiments and Fractal Analysis," in *Kinematics and Dynamics of Lava Flows*. Editors M. Manga and G. Ventura (Boulder: Geol. Soc. Am. Sp. Pap.), 396, 147–161. doi:10.1130/0-8137-2396-5.147

Aoki, H., and Ossaka, J. (1974). *A Mystery of Submarine Volcanoes – the Exploration Records of Nishinoshima (Kaiteikazan No Nazo)*. Tokyo: Tokai Univ. Press, 250. in Japanese.

Arrighi, S., Principe, C., and Rosi, M. (2001). Violent Strombolian and Subplinian Eruptions at Vesuvius during post-1631 Activity. *Bull. Volcanol.* 63, 126–150. doi:10.1007/s004450100130

Baba, K., Tada, N., Ichihara, H., Hamano, Y., Sugioka, H., Koyama, T., et al. (2020). Two Independent Signals Detected by Ocean Bottom Electromagnetometers during a Non-eruptive Volcanic Event: Ogasawara Island Arc Volcano, Nishinoshima. *Earth Planets Space* 72, 112. doi:10.1186/s40623-020-01240-z

Bas, M. J. L., Maitre, R. W. L., Streckeisen, A., and Zanettin, B. (1986). IUGS Subcomission on the Systematics of Igneous RocksA Chemical Classification of Volcanic Rocks Based on the Total Alkali-Silica Diagram. *J. Petrology* 27, 745–750. doi:10.1093/petrology/27.3.745

Blake, S., and Bruno, B. C. (2000). Modelling the Emplacement of Compound Lava Flows. *Earth Planet. Sci. Lett.* 184, 181–197. doi:10.1016/s0012-821x(00)00278-8

Calvari, S., Neri, M., and Pinkerton, H. (2002). Effusion Rate Estimations during the 1999 summit Eruption on Mount Etna, and Growth of Two Distinct Lava Flow fields. *J. Volcanol. Geotherm. Res.* 119, 107–123. doi:10.1016/S0377-0273(02)00308-6

Cavallaro, D., and Coltelli, M. (2019). The Graham Volcanic Field Offshore Southwestern Sicily (Italy) Revealed by High-Resolution Seafloor Mapping and ROV Images. *Front. Earth Sci.* 7, 311. doi:10.3389/feart.2019.00311

Cimarelli, C., Costa, A., Mueller, S., and Mader, H. M. (2011). Rheology of Magmas with Bimodal crystal Size and Shape Distributions: Insights from Analog Experiments. *Geochem. Geophys. Geosyst.* 12, a–n. doi:10.1029/2011GC003606

Cronin, S., BrennaSmith, M. I. E. M., Smith, I., Barker, S., Tost, M., Ford, M., et al. (2017). New Volcanic Island Unveils Explosive Past. *Eos* 98, 1. doi:10.1029/2017EO076589

Di Traglia, F., Cimarelli, C., de Rita, D., and Gimeno Torrente, D. (2009). Changing Eruptive Styles in Basaltic Explosive Volcanism: Examples from Croscat Complex Scoria Cone, Garrotxa Volcanic Field (NE Iberian Peninsula). *J. Volcanology Geothermal Res.* 180, 89–109. doi:10.1016/j.jvolgeores.2008.10.020

Edmonds, M. (2008). New Geochemical Insights into Volcanic Degassing. *Phil. Trans. R. Soc. A.* 366, 4559–4579. doi:10.1098/rsta.2008.0185

Fiske, R. S., Cashman, K. V., Shibata, A., and Watanabe, K. (1998). Tephra Dispersal from Myojinsho, Japan, during its Shallow Submarine Eruption of 1952-1953. *Bull. Volcanology* 59, 262–275. doi:10.1007/s004450050190

Giordano, D., Russell, J. K., and Dingwell, D. B. (2008). Viscosity of Magmatic Liquids: a Model. *Earth Planet. Sci. Lett.* 271, 123–134. doi:10.1016/j.epsl.2008.03.038

Gonnermann, H. M., and Manga, M. (2013). in *"Dynamics of Magma Ascent in the Volcanic Conduit," in* Modeling Volcanic Processes. Editor S. A. Fagents, T. K. P. Gregg, and R. M. C. Lopes (Cambridge University Press), 55–84.

Griffiths, R. W., and Fink, J. H. (1992). Solidification and Morphology of Submarine Lavas: a Development on Extrusion Rate. *J. Geophy. Res.* 97, 19729–19737. doi:10.1029/92jb01594

Griffiths, R. W. (2000). The Dynamics of Lava Flows. *Annu. Rev. Fluid Mech.* 32, 477–518. doi:10.1146/annurev.fluid.32.1.477

Gualda, G. A. R., Ghiorso, M. S., Lemons, R. V., and Carley, T. L. (2012). Rhyolite-MELTS: A Modified Calibration of MELTS Optimized for Silica-Rich, Fluid-Bearing Magmatic Systems. *J. Petrology* 53, 875–890. doi:10.1093/petrology/egr080

Harris, A. J. L., Dehn, J., and Calvari, S. (2007). Lava Effusion Rate Definition and Measurement: a Review. *Bull. Volcanol.* 70, 1–22. doi:10.1007/s00445-007-0120-y

Hon, K., Kauahikaua, J., Denlinger, R., and Mackay, K. (1994). Emplacement and Inflation of Pahoehoe Sheet Flows: Observations and Measurements of Active Lava Flows on Kilauea Volcano, Hawaii. *Geol. Soc. Am. Bull.* 106, 351–370. doi:10.1130/0016-7606(1994)106<0351:eaiops>2.3.co;2

Houghton, B. F., and Gonnermann, H. M. (2008). Basaltic Explosive Volcanism: Constraints from Deposits and Models. *Geochemistry* 68, 117–140. doi:10.106/j.chemer.2008.04.00210.1016/j.chemer.2008.04.002

Huppert, H. E., Shepherd, J. B., Haraldur Sigurdsson, R., and Sparks, S. J. (1982). On Lava Dome Growth, with Application to the 1979 Lava Extrusion of the Soufrière of St. Vincent. *J. Volcanology Geothermal Res.* 14, 199–222. doi:10.1016/0377-0273(82)90062-2

Ishizuka, O., Taylor, R. N., Yuasa, M., Milton, J. A., Nesbitt, R. W., Uto, K., et al. (2007). Processes Controlling Along-Arc Isotopic Variation of the Southern Izu-Bonin Arc. *Geochem. Geophys. Geosyst.* 8, 6Q06008. doi:10.1029/2006gc001475

James, M. R., Lane, S. J., and Houghton, B. F. (2013). "Unsteady Explosive Activity: Strombolian Eruptions," in *Modeling Volcanic Processes*. Editor S. A. Fagents, T. K. P. Gregg, and R. M. C. Lopes (Cambridge University Press), 107–128.

Kaneko, T., Maeno, F., Yasuda, A., Takeo, M., and Takasaki, K. (2019). The 2017 Nishinoshima Eruption: Combined Analysis Using Himawari-8 and Multiple High-Resolution Satellite Images. *Earth Planets Space* 71, 140. doi:10.1186/s40623-019-1121-8

Kilburn, C. R. J., and Lopes, R. M. C. (1988). The Growth of Aa Lava Flow fields on Mount Etna, Sicily. *J. Geophys. Res.* 93, 14759–14772. doi:10.1029/jb093ib12p14759

Lescinsky, D. T., and Sisson, T. W. (1998). Ridge-forming, Ice-Bounded Lava Flows at Mount Rainier, Washington. *Geology* 26, 351–354. doi:10.1130/0091-7613(1998)026<0351:rfiblf>2.3.co;2

Maeno, F., Nakada, S., and Kaneko, T. (2016). Morphological Evolution of a New Volcanic Islet Sustained by Compound Lava Flows. *Geology* 44, 259–262. doi:10.1130/G37461.1

Maeno, F., Nakano, S., Yoshimoto, M., Ohminato, T., Watanabe, A., Kawakami, K., et al. (2017). First landing and Survey of a New Volcanic Island: Nishinoshima. *J. Geogr. (Chigaku Zasshi)* 126, N1–N13. in Japanese with English abstract.

Maeno, F., and Taniguchi, H. (2006). Silicic Lava Dome Growth in the 1934-1935 Showa Iwo-Jima Eruption, Kikai Caldera, South of Kyushu, Japan. *Bull. Volcanol.* 68, 673–688. doi:10.1007/s00445-005-0042-5

Maeno, F., Yasuda, A., Nakano, S., Yoshimoto, M., Ohminato, T., Watanabe, A., et al. (2018). Formation Process of a New Volcanic Island at Nishinoshima, Ogasawara, Japan, Inferred from Eruptive Products. *J. Adv. Mar. Sci. Tech. Soc.* 24, 35–44. doi:10.14928/amstec.24.1_35 in Japanese with English abstract.

Maeno, F., and Yoshimoto, M. (2020). Characteristics and Change of Geomorphology, Geology and Eruptive Materials in the Eruption of Nishinoshima Volcano, Ogasawara. *Ogasawara Res.* 46, 37–51. in Japanese with English abstract.

Morimoto, R., and Ossaka, J. (1955). The 1952-1953 Submarine Eruption of the Myojin Reef Near the Bayonnaise Rocks, Japan. *Bull. Earthq. Res. Inst. Tokyo Univ.* 33, 221–250.

Murphey, D., Sparks, R. S. J., Barclay, J., Carroll, M. R., and Brewer, D. T. S. (2000). Remobilization of Andesite Magma by Intrusion of Mafic Magma at the Soufriere Hills Volcano, Montserrat, West Indies. *J. Petrol.* 41, 21–42. doi:10.1093/petrology/41.1.21

Nakada, S., Nagai, M., Kaneko, T., Nozawa, A., and Suzuki-Kamata, K. (2005). Chronology and Products of the 2000 Eruption of Miyakejima Volcano, Japan. *Bull. Volcanol.* 67, 205–218. doi:10.1007/s00445-004-0404-4

Nakada, S., Shimizu, H., and Ohta, K. (1999). Overview of the 1990-1995 Eruption at Unzen Volcano. *J. Volcanology Geothermal Res.* 89, 1–22. doi:10.1016/s0377-0273(98)00118-8

Ohminato, T., and Watanabe, A. (2020). Seismic and Infrasound Observation at Nishinoshima Island in 2019. *Ogasawara Res.* 46, 53–68. in Japanese with English abstract.

Omori, F. (1916). *The Sakura-jima Eruptions and Earthquakes III. Bulletin of the Imperial Earthquake Investigation Committee 8*, 181–321.

Ossaka, J. (1975). Activity of Nishinoshima Volcano and its Observation (2). *GSJ Chishitsu News* 246, 1–9. in Japanese.

Ossaka, J. (1991). *Eruptions of Submarine Volcanoes in the Sea Near Japan*. Tokyo: Tokai University Press, 279. in Japanese.

Ossaka, J., Ohira, Y., and Minato, I. (1974). On the Submarine Eruption of Nishinoshima (3). *Bull. Volcanol. Soc. Jap.* 19, 37–38. in Japanese.

Parfitt, E. A. (2004). A Discussion of the Mechanisms of Explosive Basaltic Eruptions. *J. Volcanology Geothermal Res.* 134, 77–107. doi:10.1016/j.jvolgeores.2004.01.002

Pioli, L., Erlund, E., Johnson, E., Cashman, K., Wallace, P., Rosi, M., et al. (2008). Explosive Dynamics of Violent Strombolian Eruptions: The Eruption of Parícutin Volcano 1943-1952 (Mexico). *Earth Planet. Sci. Lett.* 271, 359–368. doi:10.1016/j.epsl.2008.04.026

Polacci, M., Corsaro, R. A., and Andronico, D. (2006). Coupled Textural and Compositional Characterization of Basaltic Scoria: Insights into the Transition from Strombolian to Fire fountain Activity at Mount Etna, Italy. *Geol* 34, 201–204. doi:10.1130/G22318.1

Putirka, K. D. (2008). Thermometers and Barometers for Volcanic Systems. *Rev. Mineralogy Geochem.* 69, 61–120. doi:10.2138/rmg.2008.69.3

Pyle, D. M., and Elliott, J. R. (2006). Quantitative Morphology, Recent Evolution, and Future Activity of the Kameni Islands Volcano, Santorini, Greece. *Geosphere* 2, 253–268. doi:10.1130/GES00028.1

Pyle, D. M. (2013). "Sizes of Volcanic Eruptions," in *The Encyclopedia of Volcanoes*. Editor H. Sigurdsson, B. Houghton, S. R. McNutt, H. Rymer, and J. Stix Second Edition (London: Academic Press), 257–264.

Rowland, S. K., Jurado-Chichay, Z., Ernst, G., and Walker, G. P. L. (2009). "Pyroclastic Deposits and Lava Flows from the 1759-1774 Eruption of El Jorullo, Mexico: Aspects of 'violent Strombolian' Activity and Comparison with Paricutin," in *Studies in Volcanology: The Legacy of George Walker International Association of Volcanology and Chemistry of the Earth's Interior Special Publication 2*. Editor T. Thordarson, S. Self, G. Larsen, S. K. Rowland, and Á. Höskuldsson (London: Geological Society of London), 105–128.

Sano, T., Shirao, M., Tani, K., Tsutsumi, Y., Kiyokawa, S., and Fujii, T. (2016). Progressive Enrichment of Arc Magmas Caused by the Subduction of Seamounts under Nishinoshima Volcano, Izu-Bonin Arc, Japan. *J. Volcanology Geothermal Res.* 319, 52–65. doi:10.1016/j.jvolgeores.2016.03.004

Schneider, J.-L. (2000). "Volcaniclastic Sedimentation in Submarine Settings: Products and Processes," in *Volcaniclastic Rocks, from Magma to Sediments*. Editors H. Leyrit and C. Montenat (Amsterdam: Gordon & Breach Science Publishers), 175–192.

Shinohara, M., Ichihara, M., Sakai, S. i., Yamada, T., Takeo, M., Sugioka, H., et al. (2017). Continuous Seismic Monitoring of Nishinoshima Volcano, Izu-Ogasawara, by Using Long-Term Ocean Bottom Seismometers. *Earth Planets SpaceSpace* 69, 159. doi:10.1186/s40623-017-0747-7

Sides, I. R., Edmonds, M., Maclennan, J., Swanson, D. A., and Houghton, B. F. (2014). Eruption Style at Kīlauea Volcano in Hawai'i Linked to Primary Melt Composition. *Nat. Geosci* 7, 464–469. doi:10.1038/ngeo2140

Smellie, J. L., Wilch, T. I., and Rocchi, S. (2013). 'A'ā Lava-Fed Deltas: A New Reference Tool in Paleoenvironmental Studies. *Geology* 41, 403–406. doi:10.1130/g33631.1

Smith, P. M., and Asimow, P. D. (2005). Adiabat_1ph: A New Public Front-End to the MELTS, pMELTS, and pHMELTS Models. *Geochem. Geophys. Geosyst.* 6, Q02004. doi:10.1029/2004GC000816

Sparks, R. S. J. (1997). Causes and Consequences of Pressurisation in Lava Dome Eruptions. *Earth Planet. Sci. Lett.* 150, 177–189. doi:10.1016/s0012-821x(97)00109-x

Stix, J., Torres, R. C., Narváez M, L., Cortés J, G. P., Raigosa, J. A., Gómez M, D., et al. (1997). A Model of Vulcanian Eruptions at Galeras Volcano, Colombia. *J. Volcanology Geothermal Res.* 77, 285–303. doi:10.1016/s0377-0273(96)00100-x

Sutawidjaja, I. S. (2006). Pertumbuhan Gunung Api Anak Krakatau Setelah Letusan Katastrofis 1883. *J. Geol. Indonesian* 1, 143–153. doi:10.17014/ijog.vol1no3.20063

Suzuki, Y., Yasuda, A., Hokanishi, N., Kaneko, T., Nakada, S., and Fujii, T. (2013). Syneruptive Deep Magma Transfer and Shallow Magma Remobilization during the 2011 Eruption of Shinmoe-Dake, Japan-Constraints from Melt Inclusions and Phase Equilibria Experiments. *J. Volcanology Geothermal Res.* 257, 184–204. doi:10.1016/j.jvolgeores.2013.03.017

Tada, N., Ichihara, H., Nakano, M., Utsugi, M., Koyama, T., Kuwatani, T., et al. (2021). Magnetization Structure of Nishinoshima Volcano, Ogasawara Island Arc, Obtained from Magnetic Surveys Using an Unmanned Aerial Vehicle. *J. Volcanology Geothermal Res.* 419, 107349. doi:10.1016/j.jvolgeores.2021.107349

Taddeucci, J., Edmonds, M., Houghton, B., James, M. R., and Vergniolle, S. (2013). "Hawaiian and Strombolian Eruptions," in *The Encyclopedia of Volcanoes*. Editor H. Sigurdsson, B. Houghton, S. R. McNutt, H. Rymer, and J. Stix Second Edition (London: Academic Press), 485–503.

Takeo, M., Ohminato, T., Maeno, F., Shinohara, M., Baba, K., Watanabe, A., et al. (2018). Geophysical Observations and landing Survey at Nishinoshima Volcano. *J. Adv. Mar. Sci. Tech. Soc.* 24, 45–56. doi:10.14928/amstec.24.1_45 in Japanese with English abstract.

Tamura, Y., Ishizuka, O., Sato, T., and Nichols, A. R. L. (2018). Nishinoshima Volcano in the Ogasawara Arc: New Continent from the Ocean? *Isl. Arc* 28, e12285. doi:10.1111/iar.12285

Tanakadate, H. (1934). Evolution of a New Volcanic Islet Near Io-Zima (Satsuma Prov.). *Proc. Imp. Acad. Jpn.* 11, 152–154.

Thorarinsson, S., Einarsson, T., Sigvaldason, G., and Elisson, G. (1964). The Submarine Eruption off the Vestmann Islands 1963-64. *Bull. Volcanol.* 27, 435–445. doi:10.1007/bf02597544

Thordarson, T., and Sigmarsson, O. (2009). "Effusive Activity in the 1963–1967 Surtsey Eruption, Iceland: Flow Emplacement and Growth of Small Lava Shields," in *Studies in Volcanology: The Legacy of George Walker International Association of Volcanology and Chemistry of the Earth's Interior Special Publication 2*. Editor T. Thordarson, S. Self, G. Larsen, S. K. Rowland, and Á. Höskuldsson (London: Geological Society of London), 53–84.

Umino, S., and Nakano, S. (2007). *Geology of the Chichijima Retto District, Quadrangle Series, 1:50,000*. Tsukuba: Geological Survey of Japan, AIST, 71. in Japanese with English abstract.

Valentine, G. A., Krier, D. J., Perry, F. V., and Heiken, G. (2007). Eruptive and Geomorphic Processes at the Lathrop Wells Scoria Cone Volcano. *J. Volcanology Geothermal Res.* 161, 57–80. doi:10.1016/j.jvolgeores.2006.11.003

Valentine, G. A., Krier, D., Perry, F. V., and Heiken, G. (2005). Scoria Cone Construction Mechanisms, Lathrop Wells Volcano, Southern Nevada, USA. *Geology* 33, 629–632. doi:10.1130/g21459ar.1

Walker, G. P. L. (1971). Compound and Simple Lava Flows and Flood Basalts. *Bull. Volcanol.* 35, 579–590. doi:10.1007/BF0259682910.1007/bf02596829

Walker, G. P. L. (1991). Structure, and Origin by Injection of Lava under Surface Crust, of Tumuli, ?lava Rises?, ?lava-Rise Pits?, and ?lava-Inflation Clefts? in Hawaii. *Bull. Volcanol* 53, 546–558. doi:10.1007/bf00298155

Wilson, L., and Head, J. W. (1981). Ascent and Eruption of Basaltic Magma on the Earth and Moon. *J. Geophys. Res.* 86, 2971–3001. doi:10.1029/jb086ib04p02971

Xu, W., Ruch, J., and Jónsson, S. (2015). Birth of Two Volcanic Islands in the Southern Red Sea. *Nat. Commun.* 6, 7104. doi:10.1038/ncomms8104

Yanagisawa, H., Iino, H., Ando, S., Takagi, A., and Oikawa, T. (2020). Violent Strombolian Eruption from June to August 2020 of Nishinoshima Island, Ogasawara Islands, Japan. *Bull. Volcanol. Soc. Jap.* 65, 119–124. in Japanese. doi:10.18940/kazan.65.4_119

Yuasa, M., Murakami, E., Saito, E., and Watanabe, K. (1991). Submarine Topography of Seamounts on the Volcanic Front of the Izu-Ogasawara (Bonin) Arc. *Bull. Geol. Surv. Jpn.* 42, 703–743.

Yuasa, M., and Nohara, M. (1992). Petrographic and Geochemical Along-Arc Variations of Volcanic Rocks on the Volcanic Front of the Izu-Ogasawara (Bonin) Arc. *Bull. Geol. Surv. Jpn.* 43, 421–426.

Conflict of Interest: The authors declare that the research was conducted in the absence of any commercial or financial relationships that could be construed as a potential conflict of interest.